THE MIDDLE AND UPPER ATMOSPHERE OF NEPTUNE

JAMES BISHOP
Computational Physics Incorporated

SUSHIL K. ATREYA
University of Michigan

PAUL N. ROMANI
NASA Goddard Space Flight Center

GLENN S. ORTON
Jet Propulsion Laboratory

and

BILL R. SANDEL and ROGER V. YELLE
University of Arizona

Observations pertaining to the middle and upper atmosphere of Neptune obtained from Earth have, until recently, been limited to hydrocarbon thermal emission spectra and refractive stellar occultations. The Voyager 2 encounter provided our first detailed look at these atmospheric regions. RSS and IRIS measurements have confirmed the $p-T$ structure near the tropopause inferred from pre-Voyager infrared measurements but have also revealed a steeper temperature gradient at smaller pressures and pronounced latitudinal variations, with tropopause temperatures in the range 50 K to 57 K. The pre-Voyager estimate of a stratospheric methane mixing ratio of 2%, more than 2 orders of magnitude in excess of the tropopause cold trap value, has been revised downward considerably (10^{-4}–10^{-3}) but oversaturation is still indicated. In contrast, Voyager measurements of stratospheric C_2H_2 and C_2H_6 abundances are in very close agreement with estimates from Earth-based observations: $\sim 6 \times 10^{-8}$ and $\sim 1.5 \times 10^{-6}$, respectively, near 0.5 mbar ($T \approx 160$ K). Vertical transport in the upper stratosphere is fairly vigorous, with eddy mixing coefficient values in the range 3 to 10×10^6 cm^2 s^{-1} near the 0.2 μbar level as determined from the UVS solar occultation data. Eddy mixing in the lower stratosphere ($p \gtrsim 2$ mbar) is sluggish by comparison, with values on the order of 1 to 3 $\times$ 10^3cm^{2}s^{-1} indicated by photochemical modeling of the infrared emission spectra. Submillimeter emissions by HCN and CO in the stratosphere, first detected in 1991, have raised new questions regarding stratospheric chemistry and transport on Neptune; modeling of the abundances of these species, in conjunction with continued photochemical modeling of hydrocarbon thermal emissions and the UVS solar occultation data, is likely to lead to a characterization of eddy mixing throughout the stratosphere and to tighter constraints on stratospheric N_2 and CH_4 mixing ratios. Other prominent modeling issues of current interest are

understanding the CH_4 oversaturation in the stratosphere, reconciling hydrocarbon photochemistry and aerosol production rates with haze observations, and explaining the departure of the thermal structure from radiative equilibrium. Measurements of the upper atmosphere are sparse compared with the middle atmosphere and all derive from Voyager. Preliminary analysis of the UVS solar occultation data indicates an exospheric temperature of 750±150 K, far higher than can be sustained by solar EUV heating alone, and an H_2 scale height near 10^{-2} μbar corresponding to a temperature of 250 K. Otherwise, only the UVS measurements of H_2 auroral emissions and He 584 Å airglow and the RSS occultation determinations of electron densities and the topside ionospheric plasma temperature have been reported to date. Analysis of data acquired by Voyager is still incomplete. Continued analysis of these data should lead in the near future to further insights into the mechanisms governing the stratospheric and thermospheric thermal structure. A longer term goal is to combine our knowledge of the thermal structure and composition with dynamical modeling of the middle atmosphere to obtain a more comprehensive picture of stratospheric energetics and to explore the coupling to the troposphere; continued groundbased and satellite observations with high spatial (latitudinal) resolution will be needed to meet this goal.

I. INTRODUCTION

The main subject of this chapter is the middle atmosphere of Neptune, referring to the region between the tropopause at an atmospheric pressure of roughly 100 mbar and the onset of the thermospheric temperature gradient at pressures of ~0.1 μbar. Emphasis is given to reviewing what is currently known about the stratospheric thermal structure and composition based on observations; the insights afforded by modeling of the various available data sets are also discussed. While our knowledge of the upper atmosphere is still fragmentary, the Voyager flyby has provided data that should eventually enable us to identify the main mechanisms governing the energetics of Neptune's thermosphere. The level adopted in this chapter for the top of the stratosphere (or stratosphere-mesosphere) is somewhat arbitrary; however, the volume mixing ratio of methane, $f(CH_4)$, is rapidly decreasing with decreasing pressure at the ~0.1 μbar level and vibrational relaxation has been reached.

The observations covered in this chapter fall into two broad categories: remote observations made from Earth and Voyager flyby measurements. Observations in the former category, principally infrared radiance spectra and refractive stellar occultations, have been carried out for about two decades. These helped prepare us for some of the Voyager flyby results and defined many of the issues that have occupied researchers in the post-Voyager era. The relevant Voyager observations were carried out with the ultraviolet spectrometer (UVS) (Broadfoot et al. 1977,1989), the infrared interferometer spectrometer (IRIS) (Hanel et al. 1977; Conrath et al. 1989), and the radio science subsystem (RSS) (Eshleman et al. 1977; Tyler et al. 1989). The wealth of data from these instruments has greatly expanded our appreciation of the Neptune atmosphere and has greatly tightened the constraints that must

be met by successful models of stratospheric thermal structure, composition, aerosols, and dynamics.

The chapters in this volume on the troposphere (Gautier et al.) and aerosols, clouds and hazes (Baines et al.) each cover topics of direct relevance to this chapter. Current estimates for the abundances of He and N_2 obtained from the Voyager RSS occultations (Tyler et al. 1989; Lindal 1992) and IRIS measurements (Conrath et al. 1989; Conrath et al. 1991*b*), and the implications of these abundances, are discussed in detail by Gautier et al. The upper tropospheric and lower stratospheric thermal structure (referring to the variation in temperature T with atmospheric pressure p), horizontal variations in the $p-T$ structure, and dynamical implications thereof, are also discussed in the troposphere chapter. Hazes formed in the lower stratosphere from condensation of stable hydrocarbons photochemically generated at higher altitudes also offer insights into stratospheric composition; observations of these hazes are discussed in the Chapter by Baines et al. The history of older groundbased observations of Neptune, typically carried out at visible and near-infrared wavelengths, is also summarized in those chapters.

The structure of this chapter is as follows. In Sec. II the observations giving direct information on the stratospheric thermal structure are discussed, and the results from groundbased stellar occultations and the Voyager UVS solar occultations are covered in some detail. A description of post-Voyager $p-T$ models utilized in analyses of composition data then follows. In Sec. III the observations pertaining to stratospheric composition are reviewed, focusing in turn on hydrocarbon abundances (CH_4, C_2H_6, and C_2H_2), evidence for spatial and temporal variations in these abundances, and HCN and CO abundances. In Sec. IV the major current topics in middle atmosphere modeling are discussed: accounting for the high observed stratospheric temperatures, explaining the apparent oversaturation abundances of methane in the lower stratosphere, predicting C_2 hydrocarbon abundances and haze production rates, understanding the strength of and vertical variation in vertical transport ("eddy mixing") implied by observed hydrocarbon abundances, and explaining the abundances of the recently detected species HCN and CO. Lastly, in Sec. V those topics pertaining to the upper atmosphere about which we have some information are addressed: thermal structure, He 584 Å dayglow, aurora and photoelectron-excited emissions, and the ionosphere.

II. MIDDLE ATMOSPHERE THERMAL STRUCTURE

Knowledge of the thermal structure is crucial to determining the composition from remote sensing observations. For the stratosphere, we now have data sets addressing three distinct pressure regimes, illustrated in Fig. 1. (Here and elsewhere in this chapter, quoted $p-T$ results have been rescaled to a helium volume mixing ratio of 0.19 unless otherwise noted.) At pressures $p \lesssim 10^{-2}$ μbar, the Voyager UVS solar occultations have provided the outlines of the thermospheric scale height structure, along with constraints on the

atmospheric scale height near 0.2 mbar (Broadfoot et al. 1989; Yelle et al. 1993). For pressures ~30 to 1 μbar, there is an extensive set of groundbased refractive stellar occultation observations (Hubbard et al. 1987; Roques et al. 1994) that can be inverted to yield temperature profiles. At deeper levels, thermal information has been obtained from remote infrared sensing and from the Voyager flyby RSS and IRIS results. The reader is also referred to Gautier et al. (see their Chapter), where the data sets pertaining to the upper troposphere and lower stratosphere are discussed more fully.

These regimes where substantial data exist are not contiguous, as is evident in Fig. 1. This, combined with the fact that the individual data sets are neither simultaneous nor collocated, compels the use of $p - T$ models when inferring stratospheric composition. This introduces modeling uncertainties into the estimation of minor species abundances, especially the hydrocarbons. While there is still considerable uncertainty in the thermal structure for pressures lower than ~1 mbar, the $p - T$ models that have been introduced in the post-Voyager era are very similar, as discussed below.

A. Lower Stratosphere

For $p \gtrsim 1$ mbar, an extensive set of groundbased measurements of Neptune's atmospheric thermal radiation at wavelengths 7 μm to 3 mm has been collected over the years. For an assumed composition, measurements of this type can be inverted to retrieve what are in essence hemispherically averaged temperature profiles down to the ~6 bar level, with the caveat that warmer areas on the observed disk are weighted more heavily (Tokunaga et al. 1983; Hildebrand et al. 1985; Moseley et al. 1985; Orton et al. 1983,1986,1987,1990). Estimating the stratospheric temperature near the 1.0 mbar level from the outgoing thermal radiation requires a parameterization for the assumed mixing ratio of methane, while below 50 mbar the thermal structure is established by H_2 collision-induced opacities (H_2–H_2, H_2–He, etc.). The Orton et al. (1990) profile in Fig. 1 shows the stratospheric portion of such a retrieval, obtained by linearly perturbing a theoretical $p - T$ profile of Appleby (1986) until the resultant model spectrum best fitted their collection of pre-Voyager data at the longer wavelengths dominated by H_2 collision-induced opacity. The tropopause at $p \approx 100$ mbar is cold enough ($T \approx 54$ K) to "cold trap" methane if supplied from below.

The Voyager RSS occultations (Tyler et al. 1989; Lindal 1992) and IRIS mapping sequences (Conrath et al. 1991*b*) carried out during the Neptune encounter have provided information on spatial scales not possible with Earth-based observations. Both experiments confirmed the existence of the thermal inversion and the placement of the cold tropopause deduced from the groundbased observations. The RSS profiles in Fig. 1 are definitive in terms of detailed vertical structure, but only pertain to specific locations on the planet at the time of encounter (60°N for ingress, 45 to 38°S for egress); thus, the slightly warmer temperatures (~2 K) near the temperature minimum retrieved from the groundbased results are probably due to a greater weighting of emis-

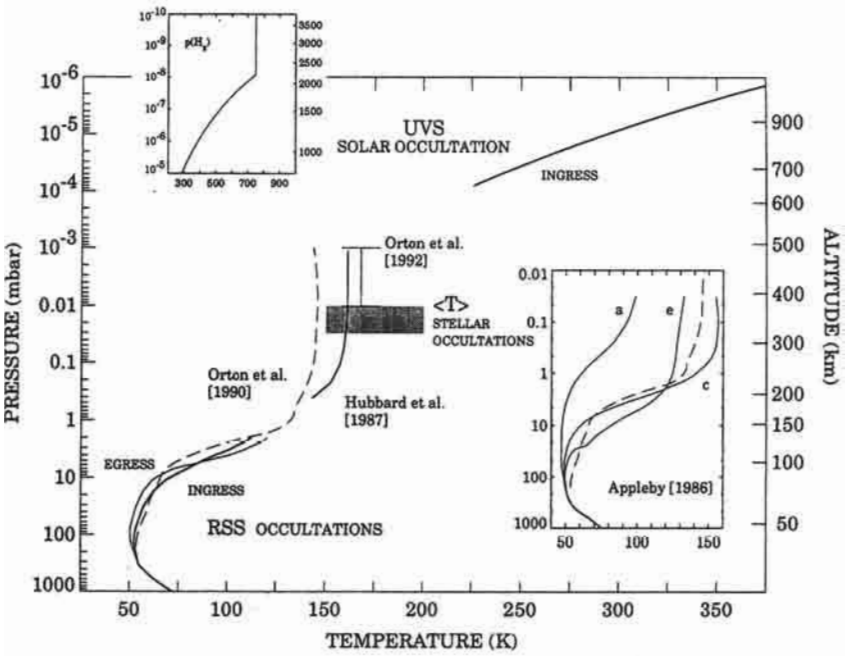

Figure 1. Selected $p-T$ results. The RSS occultations (Lindal 1992) provide the main data set for pressures $p \gtrsim 2$ mbar. Refractive stellar occultation lightcurves typically yield temperature retrievals at pressures 1 to 30 μbar; the 20 August 1985 occultation analyzed by Hubbard et al. (1987) exhibited a central flash, permitting the construction of a plausible $p-T$ profile down to 0.4 mbar. The shaded region in this figure corresponds to the range of mean temperatures $\langle T \rangle$ defined by numerous stellar occultation inversions (see text). The Orton et al. (1990) profile (f(He) = 0.15) is based on perturbations of the radiative convective models of Appleby (1986); the a, c, and e Appleby models are shown in the inset (f(He)/f(H_2) = 0.1), where the Orton et al. (1990) profile is reproduced. Orton et al. (1992) derived a mean temperature 168±10 K near 1 to 10 μbar from spectral fits for the CH_3D/CH_4 ratio (see text). At higher altitudes, H_2 densities and scale heights in the 10^{-2} μbar region have been inferred from the UVS ingress solar occultation data (Broadfoot et al. 1989); their H_2 partial pressure profile for the upper thermosphere is shown in the upper inset. The altitude scale at the right is for a model atmosphere constructed using the ingress RSS (Hubbard et al. 1987), and ingress UVS profiles, referenced to the 1 bar level. (Unless otherwise noted, f(He) = 0.19 is assumed.)

sions from warmer tropopause regions not sampled by the RSS occultations (refer to Fig. 4 of the Chapter by Gautier et al.).

Combined analysis of the RSS and IRIS data has also provided an estimate of 0.19±0.032 for the helium mixing ratio (Conrath et al. 1991*a*); this is adopted as the reference value in this chapter. Subsequent analysis (Conrath et al. 1993), motivated by the recent discovery of HCN in the lower stratosphere of Neptune (Marten et al. 1991; Rosenqvist et al. 1992), has

indicated that N_2 mixing ratios as large as 0.006 are admitted by the IRIS data. For $f(N_2) = 0.003$, the mean molecular weight m_{atm} of 2.393 inferred by Conrath et al. (1991*a*) implies a reduction in the implied He mixing ratio to 0.15. Cosmogonic implications are discussed in the Chapter by Gautier et al. As regards stratospheric studies, the main role of He and N_2 (aside from the potential role played by N_2 in the generation of stratospheric HCN) is in establishing the value of m_{atm} which directly impacts temperature determinations; at present, there seems to be no reason to expect significant revisions in the currently accepted value.

An additional constraint on the stratospheric temperature has been put forward by Orton et al. (1992). Their moderate and high-resolution infrared data (Sec. III) at wavenumbers 1100 to 1300 cm^{-1} in the ν_4 CH_4 and ν_6 CH_3D emission bands were separately analyzed and were found to be consistent for a mean stratospheric temperature of 168±4 K (with $[CH_3D]/[CH_4] = 3.6(\pm 0.5) \times 10^{-4}$). The nominal pressure range for this result is 1 to 10 μbar. Orton et al. give a total uncertainty of ±10 K (Fig. 1), thereby encompassing the temperature and methane mixing ratio results of Hubbard et al. (1987), Bishop et al. (1992), and Yelle et al. (1993).

B. Stellar Occultations

Numerous events have been observed since 1980, often with more than one station monitoring the same occultation (French et al. 1983,1985; Hubbard et al. 1985,1987; Roques et al. 1994). Prior to 1980, there is the BD-17°4388 event of 1968 (Kovalevsky and Link 1969; Freeman and Lyngå 1970). In an occultation of this type, the refractive dimming on immersion and brightening on emersion of the stellar light within a designated filter passband (usually the K-band at 2.2 μm) is recorded as the star passes behind the target planet as seen from Earth. Observations of an occultation by several stations are particularly valuable by allowing a search for possible latitudinal or longitudinal variations, because the chords defined by the track of the star behind the target planet will intersect the limb at different locations. If the measured lightcurve I/I_o is of sufficient quality, it can be inverted using established techniques to yield a vertical refractivity profile (Wasserman and Veverka 1973; Vapillon et al. 1973; Hunten and Veverka 1975; French et al. 1978). Then, if enough is known regarding the composition to specify the refractive index and mean molecular weight, the refractivity profile can be converted to a gas density profile and the $p - T$ profile derived using the hydrostatic equation and the ideal gas law. Sometimes, however, the measurement is not suitable for inversion and one must rely on fitting to an isothermal form (Baum and Code 1953). Generally speaking, for pressures near 10 μbar, the temperature profiles retrieved in the inversion process are somewhat uncertain (~10%) as to the mean temperature, but the temperature variations within a profile are considered to be more reliable.

The occultation modeling of Hubbard et al. (1987) has been influential in the analysis of recent measurements of hydrocarbon abundances in the

stratosphere of Neptune. The central flash observed at CTIO and ESO in Chile during the 20 August 1985 occultation suggested a temperature of 143 K (albeit a temperature averaged around the apparent limb) near 0.42 mbar, overlapping the pressure regime wherein C_2H_2 and C_2H_6 infrared emissions escaping the atmosphere arise. By modeling the central flash and limb data both separately and together, Hubbard et al. were able to estimate the errors associated with astrometric coordinates, apparent oblateness and equatorial radius at 1 μbar, etc. The data lightcurves were fitted to a modified Baum-Code equation prior to inversion, however, so the $p - T$ profiles presented in Fig. 4 of Hubbard et al. (see Fig. 1) do not represent true inversions of the intensity data as Hubbard et al. note. Instead, their objective was to show that the central flash data could be fitted with a plausible temperature distribution without invoking absorption by methane as was done in an earlier analysis of the same data (Lellouch et al. 1986).

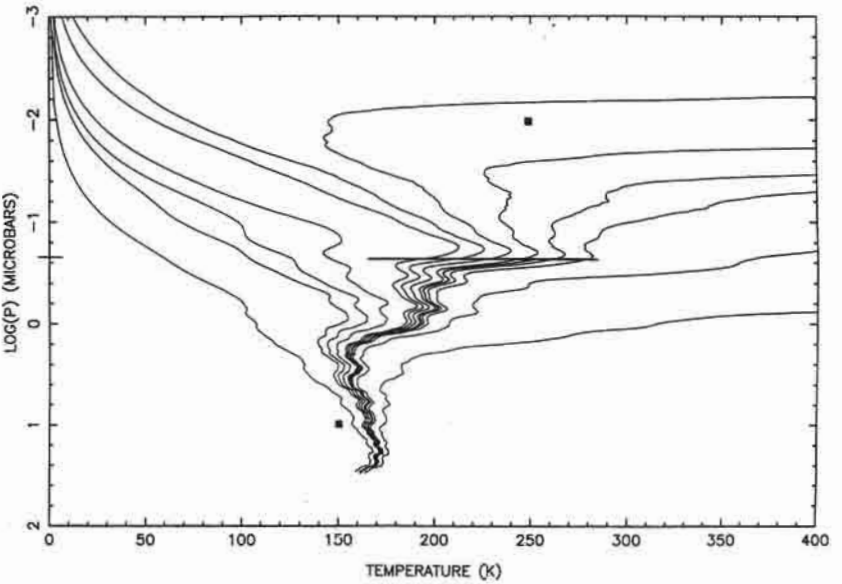

Figure 2. Family of solutions obtained from inversion of the 20 August 1985 stellar occultation immersion data obtained at the European Southern Observatory. The discrete $p - T$ points (solid squares) are from the preliminary UVS analysis of Broadfoot et al. (1989) (figure taken from Roques et al. 1994).

Roques et al. (1994) have carried out the most comprehensive study to date of stellar occultations by the Neptune atmosphere. Roques et al. collected and analyzed 22 occultation profiles obtained from 9 separate occultation events (1983–1990), some previously published, with the goal of deriving a homogeneous set of $p - T$ profiles for the upper stratosphere. The suboccultation points of the collected lightcurves span the latitude range 70°S

to 45°N without any strong evidence for a recognizable latitudinal or solar insolation variation; however, a clustering of higher average temperatures $\langle T \rangle$ near 20°S was noted and the distinctly nonisothermal profiles seem restricted to near-equatorial latitudes. Because an inversion method yields a field of solutions, an independent criterion must be found for choosing a particular profile from among the possible divergent solutions. In addition, retrieved temperature profiles are exponentially sensitive to errors as higher levels are probed, so temperatures for $p < 1$ μbar are increasingly less reliable. An example of a family of inversion profiles from the ESO immersion data from 20 August 1985 is shown in Fig. 2. To facilitate the comparison of inversion profiles from their data sets, Roques et al. arbitrarily selected those $p - T$ profiles that retained small-scale structure to as high an altitude as possible because the small-scale features were felt to be real. The associated "confidence interval" for retrieved temperatures using this criterion is 130 K wide at 0.2 μbar (Fig. 2) but shrinks to 5 K near the 10 μbar level. The option of using an initial $p - T$ point derived from the UVS solar occultation results presented by Broadfoot et al. (1989), e.g., the estimate of 250 K at 10^{-2} μbar, was decided against because of the strong indications in the stellar occultation data that Neptune's stratospheric temperature structure is highly variable in time and location. For each of the 22 invertible lightcurves, Roques et al. defined a mean temperature $\langle T \rangle$ by averaging their inversion results over the 10 to 30 μbar range where the $p - T$ profiles are least sensitive to initial conditions and uncertainties in flux levels. These are shown in Fig. 3, where the enhanced temperatures near 20°S noted earlier can be seen. A fairly wide range of temperatures is indicated: $150\ \text{K} \lesssim \langle T \rangle \lesssim 200\ \text{K}$ (Fig. 1).

Based on a comparison of the apparent temporal variation in $\langle T \rangle$ with variations in occultation-derived averaged temperatures for the Uranus stratosphere and in solar activity indices, Roques et al. (1994) have suggested that the averaged stratospheric temperature on Neptune exhibits a solar cycle variation of magnitude ~50 K with a time lag of roughly one year. However, many more observations are needed to confirm this proposed trend.

C. Voyager UVS Solar Occultations

A preliminary analysis of Voyager UVS data on Neptune's thermal structure is presented by Broadfoot et al. (1989) and a more detailed analysis of limited altitude regions is given in Yelle et al. (1993). The UVS solar occultation experiment can provide information on the thermal structure when extinction is caused predominantly by H_2. As the major atmospheric constituent, H_2 must be in hydrostatic equilibrium, implying that measurements of the variation of density with altitude may be used to infer temperature. H_2 is the dominant absorber in the atmosphere in three separate wavelength ranges. At wavelengths below 800 Å, extinction in the atmosphere is due primarily to absorption by H_2 in its ionization continuum. The cross section for this process is large and consequently these wavelengths probe the upper thermosphere where pressures are on the order of 10^{-5} μbar. From 800 to 1100 Å, extinc-

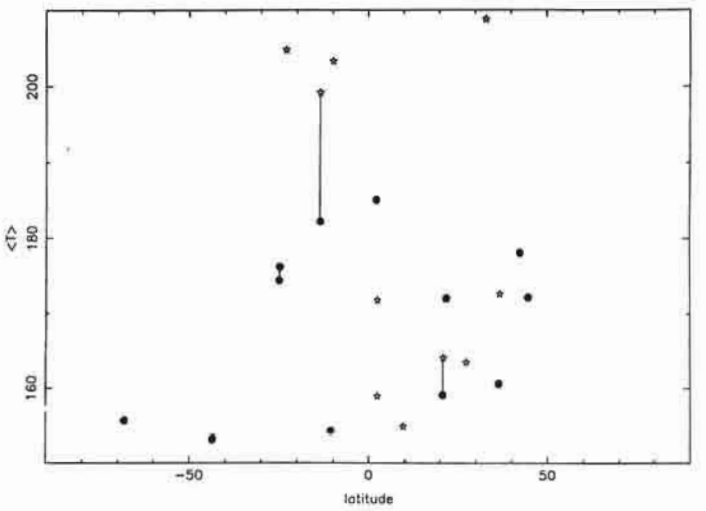

Figure 3. Variation of the mean temperature $\langle T \rangle$ at 10 to 30 μbar vs latitude of the suboccultation point, obtained from 22 stellar occultation lightcurves spanning 1983 to 1990. Temporal variations may also be involved. Points represented by filled circles correspond to higher quality data; lines in this figure connect points corresponding to data obtained from nearby sites (figure taken from Roques et al. 1994).

tion is caused primarily by absorption in the electronic band systems of H_2. These wavelengths probe the atmosphere over a large region centered about 10^{-2} μbar. At wavelengths longward of 1500 Å, Rayleigh-Raman scattering by H_2 is a dominant extinction process. The cross section for Rayleigh-Raman scattering is $\sim 10^{-24}$ cm^2 and pressures on the order of 0.2 mbar are probed.

The region from 250 to 650 km above the 1 bar level appears to be dominated by hydrocarbon rather than H_2 absorption and inferences on the thermal structure are impossible. Although the altitude distribution of hydrocarbons is interesting in its own right, we are forced to rely upon interpolation and other types of constraints for the 250 to 650 km altitude region. Theoretical models, to be discussed briefly in Sec. IV.A, offer little guidance because they have not been able to reproduce the observed thermal structure.

The geometrical characteristics of the UVS solar occultations are listed in Table I. In general, results from the ingress and egress occultations are remarkably similar, especially for the thermal structure. The UVS data require significant processing to obtain useful sets of transmission spectra as a function of altitude. The data reduction techniques are documented in Yelle et al. (1993) and the reader is referred to this paper for a detailed discussion.

Figure 4 shows the H_2 densities inferred by Yelle et al. (1993) from the H_2 band absorption and the Rayleigh-Raman extinction data. Densities are plotted against altitude above the 1 bar radius at the occultation latitude using values of 24,445 km and 24,535 km for ingress and egress (Lindal

TABLE I

UVS Solar Occultation Parameters

Parameter	Entrance	Exit
Spacecraft event time	89–237/04:00	89–237/04:53
Encounter relative time	00:00	+00:53
Geographic location	61°N, 259°W	49°S, 160°W
Range to center of Neptune (km)	2.96×10^4	8.00×10^4
Slant range to tangent point (km)	1.42×10^4	7.56×10^4
dz/dt (km s^{-1})	−9.9	12.8
Size of Sun in atmosphere (km)	4.1	22

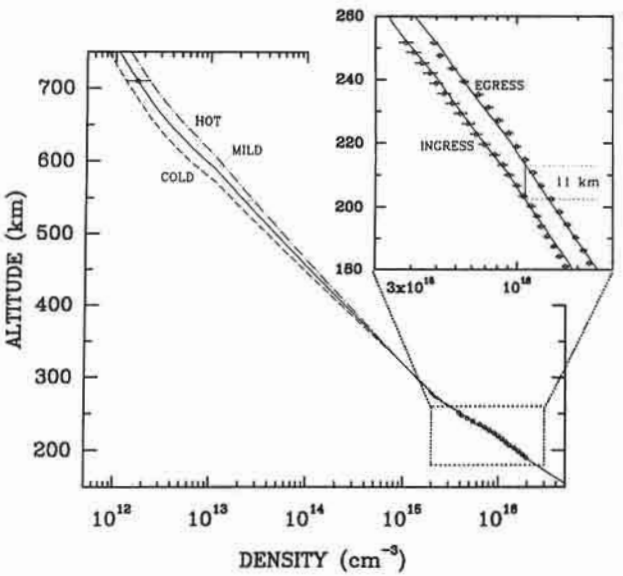

Figure 4. H_2 densities determined by Yelle et al. (1993) from the UVS egress solar occultation data in the 180 to 280 km region and the density at 710 km determined from the H_2 electronic band absorptions. Also shown are the H_2 densities for their $p - T$ models. The insert shows a comparison of ingress and egress results.

1992). If these radii are correct then there is a difference in H_2 density between ingress and egress in the 180 to 260 km region. If expressed as an altitude shift the density difference amounts to 11 km. Results from the RSS experiment at these altitude levels are intermediate between the UVS ingress and egress results with equivalent densities lying about 3 km above the UVS ingress results and 8 km below the UVS egress results. These small altitude differences could be due to inaccuracies in our knowledge of the shape of Neptune at 1 bar or to latitudinal variations in thermal structure between 1 bar and ~180 km. It is important to note that although the density differences appear to be real in the sense that they are larger than the error bars, all three results (UVS ingress, egress, and RSS) agree to within 25%.

The densities near 700 km, where extinction is due to absorption in the electronic bands of H_2, are more problematical. To date, it has proved impossible to achieve an adequate fit between observations and models of the absorption spectra. Figure 5 shows measured and calculated absorption spectra illustrating this problem. Models that match the observed spectra above 1000 Å exhibit too much transmission at shorter wavelengths. The electronic bands of H_2 are fairly well understood and it is unlikely that the discrepancy is due to inaccurate molecular data.

Yelle et al. (1993) chose to rely upon the 1000 to 1050 Å region to infer H_2 densities from the transmission spectra. They argued that the transmission

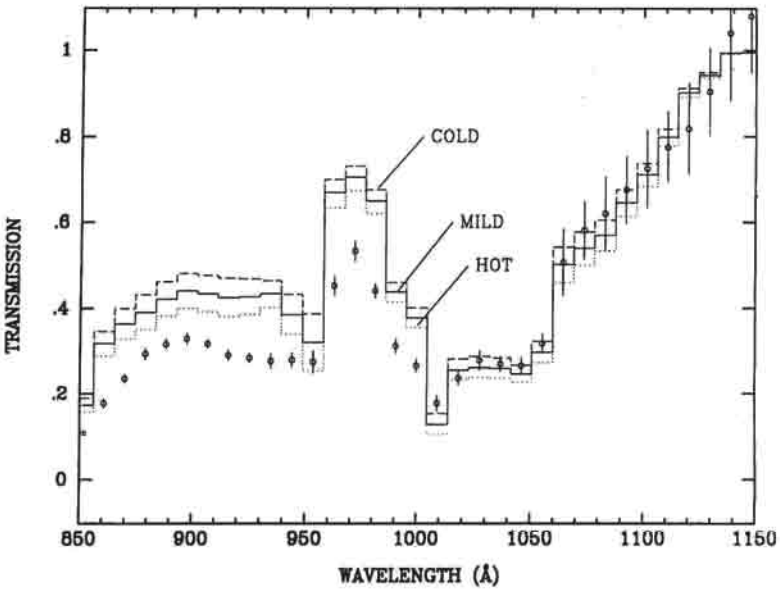

Figure 5. The transmission spectrum in the H_2 electronic band spectral region at 710 km tangent height recorded by the UVS instrument during the egress solar occultation, compared with model fits (Yelle et al. 1993). The region near 102.5 nm (H Lyman β) was used to infer the H_2 density.

properties of the atmosphere can be modeled accurately at these wavelengths because the only important process is absorption of the solar H Lyman β line by the 6-0 band of the H_2 Lyman system. In addition, because the solar H Lyman β line is strong, systematic errors in the data reduction should be less important from 1000 to 1050 Å. If this reliance upon the 1000 to 1050 Å region is correct then the H_2 density at 700 km is determined to within a factor of 2, as shown in Fig. 4. The 11 km shift discovered in the Rayleigh-Raman data also appears in the H_2 electronic band data when observed spectra are compared. Thus, the thermal structure between 200 and 700 km appears to be similar at the ingress and egress locations.

D. Empirical $p - T$ Models

As noted earlier, the available data do not provide a complete, contiguous stratospheric $p - T$ profile. The Voyager encounter results have been used to construct provisional models needed in the analysis of data on minor species distributions (Bézard et al. 1991; Bishop et al. 1992; Orton et al. 1992; Yelle et al. 1993). These models all adopt the RSS profiles at pressures deeper than ~1.0 mbar and all treat the 1.0 μbar temperature as a free parameter for the mean temperature at pressures ~100 to 1 μbar. In addition, the Voyager constraints on the helium mixing ratio (Conrath et al. 1991*a*) and the reduction in pre-Voyager estimates of the abundance of methane in the

stratosphere have been used when rescaling pre-Voyager stellar occultation and infrared sounding results; the $p - T$ profile of Hubbard et al. (1987) has been prominent in most of these models.

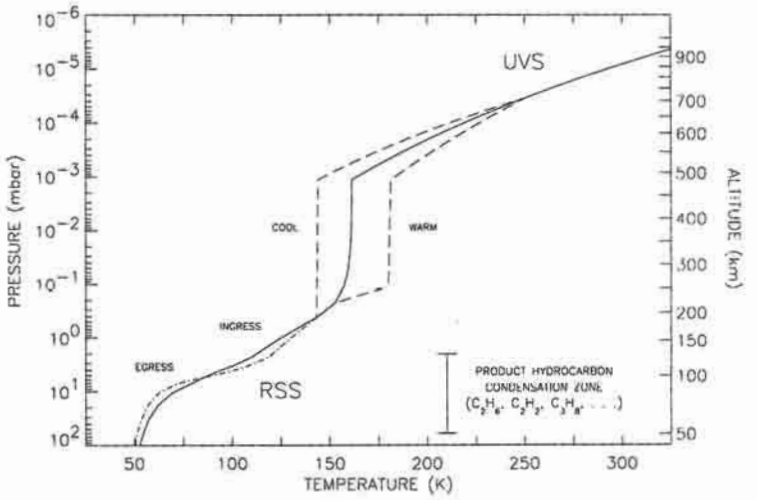

Figure 6. $p - T$ models for the Neptune stratosphere based on the RSS results for p>1.0 mbar (Lindal 1992), the ingress thermosphere model of Broadfoot et al. (1989) (p<0.03 μbar), and the Hubbard et al. (1987) profile at intermediate pressures. The cool and warm models illustrate the range of temperatures inferred from stellar occultations at a nominal pressure of 1.0 μbar. The altitude axis refers to the nominal ingress model atmosphere; the 1 bar radii as placed by the RSS occultations are 24,445 km (ingress, 61°N) and 24,535 km (egress, 49°S) (Lindal 1992). The region where photochemically produced hydrocarbons are predicted to condense (Moses et al. 1992; Romani et al. 1993) is also indicated (figure adapted from Bishop et al. 1992).

In Fig. 6, the ingress models constructed by Bishop et al. (1992) are shown, along with the nominal egress model. The nominal models used $T/T_\circ = (p/p_\circ)^\alpha$ interpolation between reference points drawn from RSS (Lindal et al. 1990), UVS (Broadfoot et al. 1989), and stellar (Hubbard et al. 1987) occultation results, rescaled to a helium mixing ratio f(He) of 0.19. The temperature at 1.0 μbar is 161 K. The nominal model adopted by Bézard et al. (1991) is closely similar to the egress model in Fig. 6, except for remaining isothermal above 1.0 μbar; their model also included a methane mixing ratio of 0.1% (m_{atm} = 2.41) resulting in a 1.0 μbar temperature of 159 K. The "warm" and "cool" $p - T$ models in Fig. 6, identified by temperatures at 1 μbar of 182 K and 144 K, respectively, reflect the range of temperatures near 1 μbar inferred from refractive stellar occultations (Fig. 1).

Orton et al. (1992) constructed a suite of models similar to those in Fig. 6,

using a perturbed average of the RSS ingress and egress $p-T$ results patched to 400 to 1 μbar temperature profiles of the form presented by Hubbard et al. (1987). The perturbation of the RSS profile was carried out using standard temperature-sounding techniques (Orton et al. 1987) to render the profile consistent with the 17 to 23 μm spectrum of Orton et al. (1990), and yielded a tropopause temperature ~2 K warmer than the averaged nominal RSS results. To encompass the range in mean temperatures derived from refractive stellar occultations (Roques et al. 1994), Orton et al. imposed 1.0 μbar temperatures ranging from 140 K to 200 K.

Yelle et al. (1993) have also developed a set of reference $p-T$ models incorporating the RSS results. Rather than use the Hubbard et al. (1987) profile, however, they chose to rely on an estimate of ~130 K for the temperature near 0.3 mbar derived from their UVS data analysis, overlaid by a rapid increase in temperature at pressures between 0.2 and 0.07 mbar and an isothermal layer at 180 K extending to the 0.1 μbar level. Thus, while drawing from UVS rather than stellar occultation results, they obtained a nominal ("mild") profile very similar in appearance to the models described above. To address uncertainties in the thermal structure, the temperature in the isothermal layer was treated as a free parameter, with cold and hot values of 170 K and 190 K, respectively. The H_2 densities in these models are shown in Fig. 4.

It is important to recognize that these models are all patchwork affairs. The Orton et al. (1992) perturbation of the RSS results, for example, arguably yields a "disk-averaged" $p-T$ profile for pressures deeper than 1.0 mbar well suited to the analysis of infrared observations, especially in that the occultation analyzed by Hubbard et al. occurred in 1985 and the Orton et al. data were acquired between 1985 and 1987 (i.e., the relevant data are roughly simultaneous). However, the RSS egress and ingress profiles differ considerably at pressures less than 100 mbar and there is no *a priori* reason to expect an averaged $p-T$ profile weighted toward the warmer tropopause regions not sampled by the RSS occultations to concur with the Orton et al. perturbed profile. Also, most of these models hinge on the 0.4 mbar point from the Hubbard et al. (1987) modified Baum-Code modeling of the 20 August 1985 central flash, and while their point was presented as being "reasonably model independent" (for a specified composition), they did not offer a complete discussion of the range in temperatures admitted by their derivation. The Hubbard et al. central flash point is in a pressure region characterized by a large vertical temperature gradient; uncertainties in the value of this gradient (or horizontal or temporal variations in this gradient) will compromise the reliability of the interpolation between the RSS results and the stellar occultation limb results needed to piece together a contiguous $p-T$ profile. Lastly, it must be noted that there is no compelling reason to believe that the stratosphere is isothermal at pressures 100 to 1 μbar. Indeed, many of the temperature profiles presented by Roques et al. (1994) are strikingly non-isothermal. However, the stratospheric composition analyses that motivated the construction of the $p-T$ profiles described above are not very sensitive

to details of the thermal structure at these pressures. In view of the lack of data pointing to long-lived nonisothermal structures, treating this layer as isothermal may be justified by more than expediency.

III. MIDDLE ATMOSPHERE COMPOSITION

The distinctive feature of the stratosphere is the photochemistry initiated by the direct absorption of solar far ultraviolet photons, with methane as the parent species. The stable disequilibrium product species C_2H_2 and C_2H_6, as well as CH_4 itself, are present in sufficient abundances that the infrared rovibronic emissions from these species dominate the 7 to 16 μm spectrum of the planet. Methane likely plays a major role in establishing the temperature structure via radiative heating and cooling (Macy and Trafton 1975; Wallace 1975; Appleby 1986,1990); ethane and acetylene may also be significant in this regard.

Infrared emissivities are, of course, very sensitive to atmospheric temperature. Voyager-derived constraints on stratospheric temperatures do not point to a single $p - T$ model, as discussed earlier; there are latitudinal variations in the Voyager results and temporal variations are suggested by the refractive stellar occultations. Nevertheless, the Voyager $p - T$ results lead to tighter constraints on minor species abundances inferred from infrared emission measurements than were available in the pre-Voyager era. We note that, in any event, a "disk-averaged" model is required for modeling the disk-integrated data typically acquired with groundbased or Earth-orbiting instruments. A thorough and very readable discussion of the earlier infrared emission measurements, their analysis and relation to models is given by Orton and Appleby (1984).

In this section, measurements providing estimates of hydrocarbon abundances are summarized first, focusing on the more recent observations. Then specific results on CH_4, C_2H_2, and C_2H_6, and the evidence for latitudinal and temporal variations are discussed. Lastly the recent submillimeter wavelength observations of HCN and CO in the Neptune stratosphere are described. Measurements related to isotopic abundances are covered in the Chapter by Gautier et al. In the following, the acronym CHES is used to denote a mixing ratio profile that is constant with height except at pressures where this exceeds the local equilibrium saturation pressure for the species in question; in such regions, the mixing ratio profile follows the equilibrium saturation pressure curve. This type of profile has been commonly used in the analysis of infrared emission data. The mixing ratio of methane in the lower stratosphere, specifically at pressures $\gtrsim$1.0 mbar (but above the nominal CH_4 condensation zone), is denoted by $f_S(CH_4)$. The methane mixing ratio expected on the basis of vapor phase saturation at the tropopause is denoted by $f_{TRAP}(CH_4)$.

A. Observations

Our first indications of the presence of hydrocarbons in the Neptune strato-

sphere came from observations of the middle infrared spectrum. An early complete spectrum (taken in 1975 and 1976) at ~2% resolution in the 8 to 13 μm region was published by Gillett and Rieke (1977), which included the broad ν_4 band of methane at 7.7 μm and the ν_9 band of ethane at 12.2 μm; independent detection of methane and ethane emission from Neptune using filter photometry was made by Macy and Sinton (1977). A better sampled and more sensitive spectrum of Neptune's disk in the 8 to 14 μm and 17 to 23 μm spectral regions at the same resolution as the Gillett and Rieke observations was obtained in 1985 (Orton et al. 1987) and was later recalibrated by Orton et al. (1990) based on further data acquired in 1986 and 1987. This spectrum, reproduced in Fig. 7, clearly shows emission by CH_4 and CH_3D at 7 to 8 μm, by C_2H_6 in the 12 μm fundamental band, by C_2H_2 in the wings of 14 μm fundamental band, and (possibly) by C_2H_4 in the 10 μm fundamental band. Kostiuk et al. (1990) observed emission in the C_2H_6 RR(4,5) line from Neptune a couple of months prior to the Voyager encounter using a very high-resolution ($\nu/\Delta\nu \approx 2.5 \times 10^5$) infrared heterodyne spectrometer; this line (840.9764 cm^{-1}) is within the 12 μm ethane band observed by Orton et al. (1987,1990) and others. Orton et al. (1992) report relatively high-resolution spectroscopic measurements ($\nu/\Delta\nu \sim 10^4$) acquired in 1989 and 1990 in several narrow intervals centered on stratospheric emission features in the 7 to 20 μm region: the 587 cm^{-1} H_2 $S(1)$ quadrupole feature, the 743 cm^{-1} $R(5)$ line of the C_2H_2 ν_5 band, the Q manifolds of C_2H_6 and $^{13}C^{12}CH_2$ near 820 cm^{-1}, and the ν_2 Q branch of CH_3D and neighboring ν_4 $P(9)$ lines of CH_4 near 1156 cm^{-1}. These results were then analyzed in conjunction with a re-analysis of the earlier results of Orton et al. (1987,1990) utilizing Voyager-derived constraints on the temperature profile and hydrocarbon abundances. Most recently, spectra at wavelengths 6.5 to 13.5 μm and 2% resolution obtained in June 1991 are discussed by Hammel et al. (1992). Results from all of these studies are effectively "disk averages" over the hemisphere facing the Earth at the time of the observations, with greater weight going to emissions from the southern hemisphere.

On the Voyager 2 spacecraft, the IRIS and UVS instruments collected data on stratospheric composition during the Neptune encounter (Conrath et al. 1989; Broadfoot et al. 1989). The IRIS measurements of the acetylene 14 μm and ethane 12 μm band emissions have been analyzed by Bézard et al. (1991); in contrast with the data acquired at Jupiter and Saturn, IRIS measurements could only establish a temperature-dependent upper limit to the methane emission because of the colder lower stratosphere of Neptune and the rapid increase in the instrumental noise equivalent spectral radiance at wavenumbers greater than 1100 cm^{-1}. Bézard et al. (1991) averaged a large selection of low-spatial resolution spectra (Fig. 8) to derive disk-averaged abundances of C_2H_2 and C_2H_6 at pressures centered near 0.5 mbar. Owing to the encounter geometry these spectra were weighted towards the southern hemisphere; the center of the field of view ranged from 10°S to 50°S. A set of spectra at higher spatial resolution showed latitudinal variations in the C_2H_2

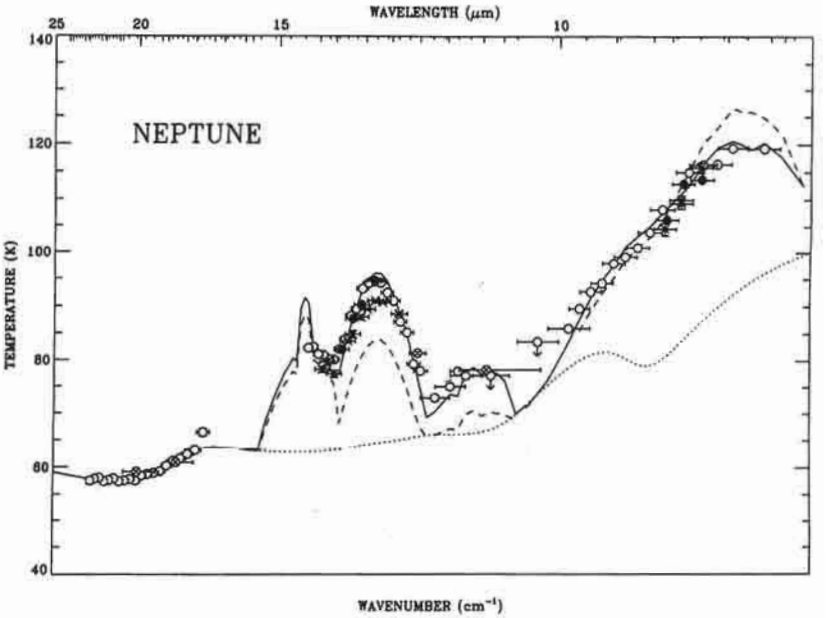

Figure 7. The 8 to 23 μm spectrum of Neptune at moderate (2%) resolution, taken from Orton et al. (1990). The data points shown as filled circles were used by Orton et al. to establish their absolute calibration; the other data points are from the following sources: Orton et al. (1987) (open circles, recalibrated), Tokunaga et al. (1983) and Orton et al. (1983) (open circles with central crosses), and Gillett and Rieke (1977) (asterisks). The earlier data sets have been rescaled for consistency with the flux standards and planetary size assumed by Orton et al. (1990). The solid line represents their "best fit" model (perturbed Appleby [1986] $p - T$ model with CHES mixing ratio profiles for C_2H_2, C_2H_6, and CH_4), while the dotted line shows the underlying spectrum arising from H_2 collision-induced opacity alone. The dashed line spectrum was calculated using hydrocarbon abundance profiles from the Romani and Atreya (1989) photochemical model.

emission (Sec. III.D). It was not possible to uncover latitudinal variations in the 12 μm ethane emission, owing to the lower signal-to-noise ratio for this feature.

The UVS solar occultation measurements at wavelengths longward of H Lyman α 121.6 nm probed the stratosphere at pressures ranging from ~0.1 μbar to ~0.1 mbar (Broadfoot et al. 1989). Both ingress (61°N latitude) and egress (49°S) occultations were recorded (Fig. 9). Dayglow and auroral measurements were also made with the UVS; these pertain to higher altitudes and are discussed in Sec. V. The solar occultation data have, to date, been the subject of two separate studies. Bishop et al. (1992), from a photochemical modeling perspective, estimated CH_4 abundances in the lower stratosphere and the strength of eddy mixing in the upper stratosphere by modeling the 125 to 138 nm lightcurves, arguing that methane was the main

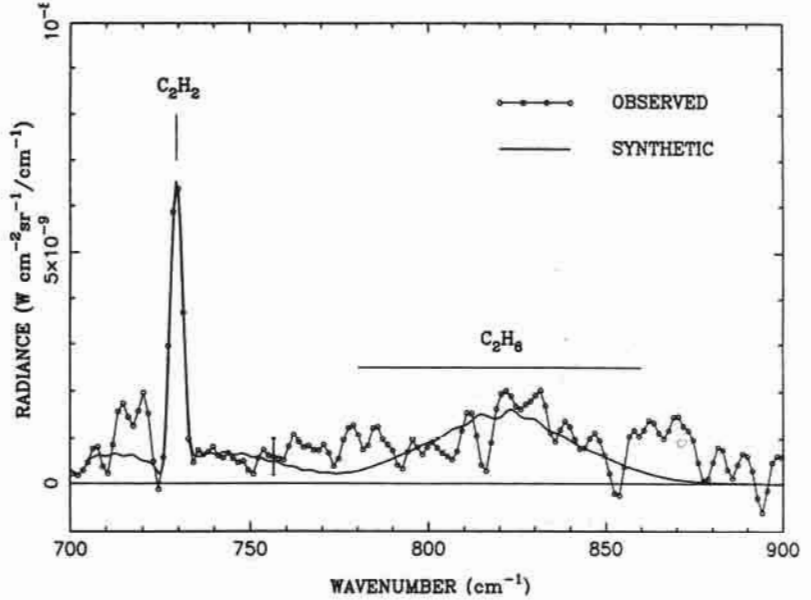

Figure 8. Disk-averaged spectrum measured by IRIS (Bézard et al. 1991) in the spectral region dominated by C_2H_2 and C_2H_6 emissions. The error bar indicates the 1-σ noise level after the disk averaging. The synthetic spectrum was computed using their nominal $p - T$ model and CHES mixing ratio profiles, with C_2H_2 and C_2H_6 mixing ratios of 6×10^{-8} and 1.5×10^{-6}, respectively.

source of opacity at these wavelengths and hence that their results were not strongly dependent on details of the photochemical modeling. Yelle et al. (1993), relying on inversion of smoothed lightcurves at wavelengths 125 to 170 nm, obtained the number density profiles for CH_4 and C_2H_6 shown in Fig. 10, along with the H_2 results shown in Fig. 4, and placed constraints on the abundances of C_2H_2 and C_2H_4.

Other observations have been used in attempts to infer hydrocarbon abundances in the Neptune stratosphere. Lellouch et al. (1986) used the apparent dimness of the central flash of the 20 August 1985 stellar occultation to infer ~1% methane mixing ratio for a strictly isothermal atmosphere (T = 150 K), but the subsequent analysis by Hubbard et al. (1987) suggested instead that the 30% decrease in mean relative central flash intensity was due to temperature gradients, as described previously. The IUE ultraviolet albedo measurements of Caldwell et al. (1988) suggested C_2H_2 mixing ratios two orders of magnitude smaller than the infrared emission analysis of Orton et al. (1987); however, the effective removal of vapor phase acetylene at pressures deeper than ~5 mbar by condensation and the presence of stratospheric aerosols were not addressed in the Caldwell et al. analysis, while the $p - T$ models used in the Orton et al. analysis were too cool (Orton et al. 1992), so that further work may yet show that the IUE and infrared data are not incompati-

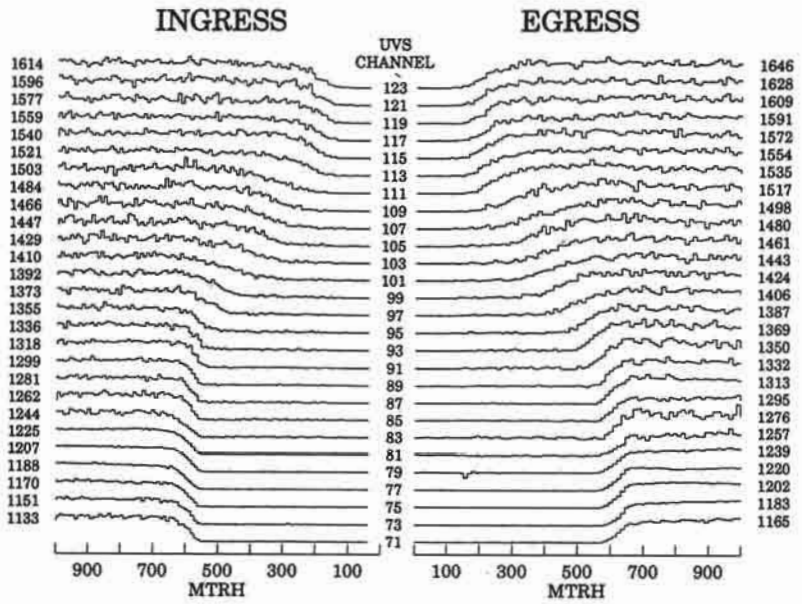

Figure 9. Subsets of the solar occultation data acquired by the Voyager UVS instrument (Broadfoot et al. 1989), shown as transmission lightcurves (I/I_o) averaged over 0.96 s intervals and ordered according to the channel center wavelengths at 500 km tangent altitude. Altitude resolutions are 9.5 km (ingress) and 12.3 km (egress), and the spectral resolution is ~2.5 nm. Wavelengths (λ) longward of H Lyman α penetrate the thermosphere: half-light points for $\lambda \lesssim 135$ nm lie at pressures 0.1 to 0.3 μbar, for 135 nm$\lesssim\lambda\lesssim$155 nm the lightcurves probe progressively deeper into the stratosphere, and for $\lambda \gtrsim 155$ nm lightcurve half-light points are near 0.2 to 0.3 mbar.

ble. Observations of stratospheric hazes offer both insights and constraints on questions regarding composition (Baines and Smith 1990; Pryor et al. 1992). For example, the location of a condensation level provides a strong clue to the identity of a condensing species, and the presence of haze aerosols can strongly affect vapor phase abundances by serving as condensation nuclei and by modifying the thermal structure. These points are discussed in the Chapter by Baines et al.

B. CH_4

The distribution of methane in the stratosphere of Neptune is primarily governed by vertical transport and loss by Lyman α photodissociation. Analysis of the Voyager UVS data (Parkinson et al. 1990; Bishop et al. 1992; Yelle et al. 1993) indicates a relatively large eddy mixing coefficient K ($\gtrsim 10^7$ cm^2 s^{-1}) in the upper stratosphere, sufficient to maintain a nearly constant CH_4 mixing ratio above its condensation level in the lower stratosphere extending to pressures $<10\,\mu$bar. Thus, use of CHES mixing ratio profiles is justified when analyzing 7.8 μm infrared emission data.

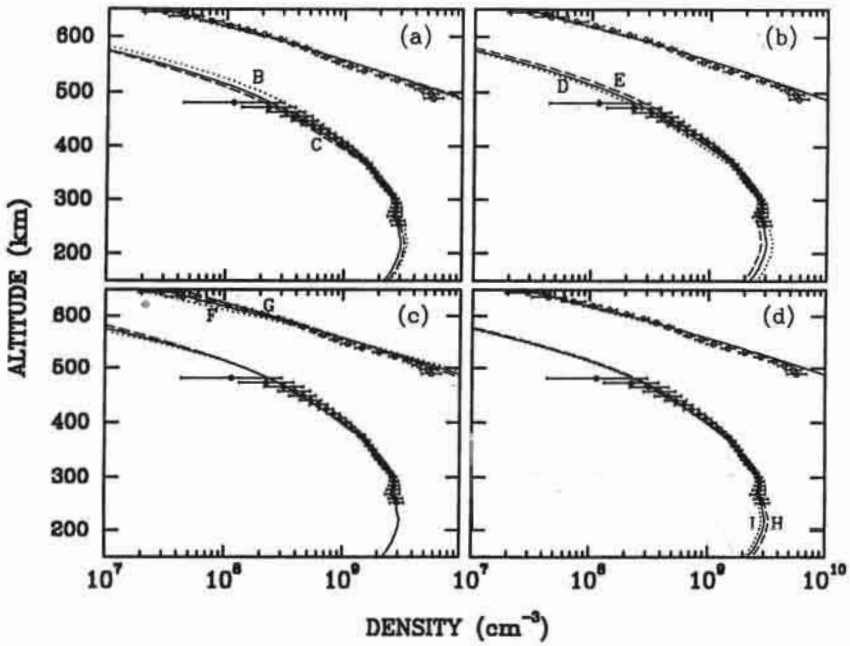

Figure 10. CH_4 and C_2H_6 number density profiles obtained by Yelle et al. (1993) from inversion of smoothed UVS egress solar occultation lightcurves. The curves are model fits characterized by eddy mixing profile, $f_S(CH_4)$ value, and the C_2H_6 production efficiency from CH_4 photolysis. The panels illustrate fits obtained by varying a designated parameter and adjusting the others to compensate: (a) CH_4 scale height at 550 km ($p \approx 0.6\,\mu$bar in their nominal $p - T$ model), 30±3 km; (b) C_2H_6 scale height at 320 km ($p \approx 30\,\mu$bar), 150±30 km; (c) z_b, the altitude at which K switches from a constant profile to a profile increasing exponentially with decreasing pressure, 300±50 km; and (d) model atmosphere, 180±10 K at 1 μbar.

The analysis of the observations reported by Orton et al. (1987,1990) relied on their perturbations of the Appleby (1986) radiative-convective equilibrium $p - T$ models (Sec. II.A) coupled with CHES mixing ratio profiles. It was found that taking $f_S(CH_4) = 0.02$ in these models worked well with this "perturbed" temperature structure to replicate the observed CH_4 emission. This value matched, but did not exceed, the 2% CH_4 mixing ratio in the troposphere inferred by Hildebrand et al. (1985) and Orton et al. (1986). Corrections for the extinction by telluric CH_4 lines, an effect not calibrated out by reference to a spectrally neutral body (e.g., a standard star), were introduced in Orton et al. (1990); such corrections are not required for C_2H_2 and C_2H_6 analysis.

Orton et al. (1992), as part of their analysis of high-resolution spectroscopy of Neptune's disk, again re-analyzed the moderate resolution CH_4 emission data. They parameterized $f_S(CH_4)$ against stratospheric temperature using the CHES profile form and $p - T$ models derived from Voyager

and refractive stellar occultation measurements (described in Sec. II.C). This analysis indicated $f_S(CH_4)$ values ranging from $2.00(\pm 0.66) \times 10^{-2}$ for a mean stratospheric temperature of 140 K to $6.88(\pm 1.74) \times 10^{-5}$ for a temperature of 200 K. Orton et al. (1992) preferred a mean stratospheric temperature of 168 ± 10 K, based on simultaneous fits to the $[CH_3D]/[CH_4]$ ratio from their moderate and high-resolution data (Sec. II.A). This temperature selection and uncertainty implies a stratospheric CH_4 mixing ratio of $7.5^{+18.6}_{-5.6} \times 10^{-4}$, giving a strong indication that $f_S(CH_4) > f_{TRAP}(CH_4)$. The 7.8 μm band intensities measured by Hammel et al. (1992) are consistent with the older Orton et al. (1987,1990) measurements, although the uncertainties in the comparison are fairly large (~40%).

Initial analysis of the UVS ingress solar occultation lightcurves (Broadfoot et al. 1989) indicated CH_4 mixing ratios $\sim 3 \times 10^{-5}$ near 0.1 μbar for a mean stratospheric temperature of 150 K. A modeling analysis of the UVS ingress and egress occultation lightcurves at wavelengths where CH_4 is expected to be the dominant source of opacity (125–138 nm) has been carried out by Bishop et al. (1992), utilizing an updated version of the Romani and Atreya (1989) photochemical code. The results of this analysis are estimates of the eddy mixing coefficient in the vicinity of the half-light levels of the 125 to 138 nm lightcurves and inferred values for the mixing ratio of methane in the lower stratosphere; these are somewhat sensitive to the choice of atmospheric $p - T$ profile and adopted eddy mixing profile but not to photochemical details. The half-light levels correspond to CH_4 mixing ratios of $\sim 5 \times 10^{-5}$, decreasing with decreasing pressure. The methane mixing ratios were mapped to the lower stratosphere via the diffusion equation, yielding $f_S(CH_4) \approx 10^{-4}$. As already indicated, there is uncertainty in this value stemming directly from our lack of knowledge of the actual $p - T$ profile at pressures 0.1 mbar $\gtrsim p \gtrsim$ 0.1 μbar, but using the $p - T$ models of Fig. 6 indicated 10^{-3} to be an effective upper limit.

Methane number density profiles obtained from the UVS egress lightcurve inversions of Yelle et al. (1993) are shown in Fig. 10. Yelle et al. derived $f_S(CH_4)$ values in the range 0.6 to 5×10^{-3} based on diffusion model fits also shown in this figure. The parameters defining these models are the $f_S(CH_4)$ value, an eddy mixing profile that has K constant at $p \gtrsim 40$ μbar and exponentially increasing for smaller pressures, and a C_2H_6 production efficiency from CH_4 photolysis (treated as a simple proportionality constant). In the fitting procedure, fluxes were estimated from the methane photolysis rate and the models were constrained to reproduce a CH_4 density of 1.3×10^9 cm^{-3} at 550 km above the 1 bar level (~0.6 μbar in their nominal $p-T$ model). The most successful fits indicate a density scale height of 30 ± 3 km for methane at this level. The range in inferred $f_S(CH_4)$ values stems largely from the range in the strength of eddy mixing at pressures greater than ~40 μbar admitted in their models. Results obtained with the UVS ingress data presented difficulties when compared with the egress results, probably stemming from systematic errors in the UVS data. Consequently, Yelle et al. restricted their

modeling to the egress density profiles. Differences with the UVS analysis results of Bishop et al. were attributed to differences in (1) the data sets used in the respective analyses; (2) modeling techniques; (3) adopted thermal profiles; and (4) the fact that the Bishop et al. analysis was restricted to the 1250 to 1380 Å region. Yelle et al. argued that this last point was probably the main source of discrepancy, in that Bishop et al. relied on photochemical modeling to estimate C_2H_6 opacities at these wavelengths and, by failing to consider the UVS data at longer wavelengths, underestimated C_2H_6 abundances at $p \approx 1$ μbar. However, underestimating ethane opacities should lead to overestimates of methane abundances, not underestimates. Differences in modeling techniques are the most likely source of discrepancy; further work on the photochemical modeling of the UVS lightcurves is needed to clarify the situation. Yelle et al. also noted that while their $f_S(CH_4)$ values appear to be consistent with values inferred from infrared measurements, there were subtle discrepancies that would require a combined analysis to resolve.

A recent re-analysis of measurements at ultraviolet and sub-micron wavelengths pertaining to stratospheric aerosol distributions (Baines and Hammel 1994) has provided simultaneous constraints on $f_S(CH_4)$ and the pressure level of the underlying tropospheric "hazetop"; this study is discussed more fully in the Chapter by Baines et al. The range of stratospheric methane abundances consistent with these data is $2 \times 10^{-5} < f_S(CH_4) < 1.7 \times 10^{-3}$ with a preferred value of 3.5×10^{-4}, in agreement with the Orton et al. (1992) 168 K result and the values derived by Bishop et al. (1992), while straddling possible $f_{TRAP}(CH_4)$ values.

C. C_2H_2 and C_2H_6

The thermal profile constraints provided by the Voyager encounter results have led to an agreement regarding "disk-averaged" C_2H_2 and C_2H_6 abundances that is in striking contrast to the CH_4 results. Utilizing CHES mixing ratio profiles, Bézard et al. (1991) retrieved from the spectrum shown in Fig. 8 an acetylene mixing ratio of $6^{+14}_{-4} \times 10^{-8}$ centered near 0.2 mbar and an ethane mixing ratio of $1.5^{+2.5}_{-0.5} \times 10^{-6}$ centered near 0.7 mbar; the nominal results are for their $p-T$ model with $T = 159$ K at 1 μbar. The largest contribution to the uncertainties is the assumed temperature uncertainty of ± 10 K. Additionally, they tested C_2H_2 and C_2H_6 mixing ratio profiles calculated with an updated version of the Romani and Atreya (1989) photochemical model, but were unable to obtain satisfactory fits for both species simultaneously.

The Kostiuk et al. (1990) analysis of groundbased heterodyne observations using pre-Voyager modeling inputs suggested that a warmer stratospheric temperature profile or a weak eddy mixing coefficient in the lower stratosphere was required to reconcile the Romani and Atreya (1989) photochemical model with observations. Both expectations have been borne out by Voyager results and updates to the photochemical model. Kostiuk et al. (1992) re-analyzed the heterodyne data employing the same modeling assumptions and inputs used by Bézard et al. This was an especially interesting exercise in that, as

described earlier, the IRIS and heterodyne spectrometer observations were nearly simultaneous, both are effectively "disk-averaged" measurements, and the emission line observed by Kostiuk et al. is within the band emission measured by IRIS. Adopting CHES mixing ratio profiles, Kostiuk et al. derived a C_2H_6 mixing ratio of $1.9(\pm 0.6) \times 10^{-6}$, where the uncertainty does not take into account temperature uncertainties. These were explored by using warm, nominal, and cool $p - T$ models taken from both Bézard et al. (1991) and Bishop et al. (1992); using the Bishop et al. $p - T$ models, the range in derived ethane mixing ratios was 1.3 to 2.4×10^{-6}. The IRIS data were also remodeled using the Bishop et al. $p - T$ models and CHES mixing ratios, yielding a range of 1.0 to 1.6×10^{-6}. The contribution functions for the IRIS and heterodyne retrievals for the nominal Bézard et al. and the extreme Bishop et al. $p - T$ models are shown in Fig. 11. Because the heterodyne observations are of higher spectral resolution than IRIS (0.0033 cm^{-1} vs 4.3 cm^{-1}), the heterodyne contribution functions peak higher and are narrower than those characterizing IRIS. This suggests the possibility of height discrimination between the results. While Kostiuk et al. (1992) found the heterodyne-retrieved ethane mole fractions were 30% higher than those of IRIS, this is within the experimental uncertainties of the two instruments and the contribution functions exhibit a large degree of overlap. Thus, it is not possible to infer a statistically significant C_2H_6 mixing ratio gradient. It is worth noting that the heterodyne observations had to be spectrally binned by a factor of 3, owing to poor signal-to-noise levels. Had this not been necessary, the contribution functions would have exhibited a smaller degree of overlap and height information could have been retrieved.

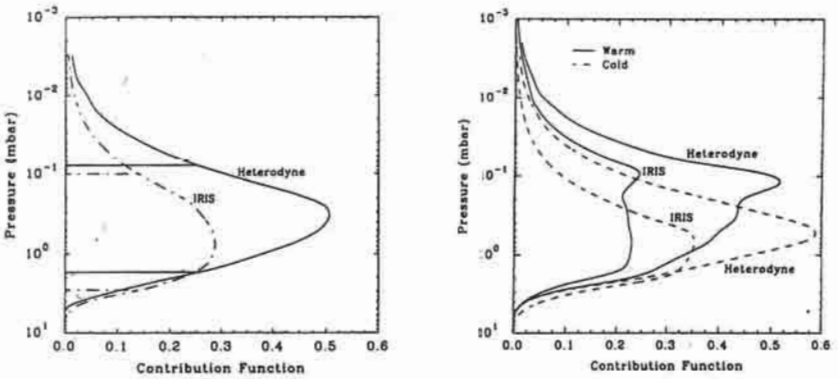

Figure 11. Contribution functions for the ethane infrared emissions measured by IRIS (Bézard et al. 1991) and by the heterodyne technique (Kostiuk et al. 1990) for CHES mixing ratio profile forms and several different $p - T$ models. The nominal $p - T$ model of Bézard et al. was used in the radiance modeling shown in the left hand panel, the bracketing "warm" and "cold" $p - T$ models of Bishop et al. were used in generating the right hand panel (figure adapted from Kostiuk et al. 1992).

Orton et al. (1992), in the course of re-analyzing their moderate resolution data (Orton et al. 1987,1990) using their previously described suite of temperature models and CHES mixing ratio profiles, obtained revised estimates for C_2H_2 and C_2H_6 abundances in the stratosphere. They briefly examined an alternative approach which replaced the assumed CHES profile form with vertical dependences of the form exhibited by the photochemical model results of Moses et al. (1992) (see Fig. 15, below); acetylene and ethane abundances for fitted profiles of this form agreed with the CHES profile results at ~0.3 mbar, near the peak of the outgoing thermal infrared radiance. The sets of solutions for the CHES models vs stratospheric temperature are shown in Fig. 12. For the nominal 168±10 K stratospheric temperature recommended by Orton et al. (1992), the maximum mixing ratios of C_2H_2 and C_2H_6 are $5.1^{+2.0}_{-4.3} \times 10^{-8}$ and $1.0^{+0.2}_{-0.8} \times 10^{-6}$, respectively. Comparison of these results with the Bézard et al. (1991) and Kostiuk et al. (1992) results shows that we have a pleasant situation in which the main sources of infrared data are completely consistent on the average abundances of the hydrocarbons C_2H_2 and C_2H_6. This implies that the calibration sources are self-consistent and the results are not systematically affected by the acquisition method or the spectral resolution. The 0.1 to 1.0 mbar averaged abundances are then determined absolutely for a given selection of the temperature profile.

In addition to C_2H_2 and C_2H_6, Orton et al. (1987) suggested that C_2H_4 emission might be responsible for the radiance observed from Neptune near 11 μm. While this was not a positive spectral identification, the maximum C_2H_4 mixing ratio required to match the spectrum was found to be 3×10^{-9} ($T \approx 138$ K). For a stratospheric temperature of 168 K, the inferred mixing ratio would be about an order of magnitude lower.

The ethane number density profiles obtained from the UVS egress light-curve inversions of Yelle et al. (1993) are shown in Fig. 10. Yelle et al. derived a C_2H_6 reference density of 2.5×10^9 cm^{-3} at 320 km (~30 μbar), which was used as a constraint in the modeling described in the previous subsection. Their most successful fits indicate a density scale height of 150±30 km for ethane at this level and C_2H_6 production efficiencies of 0.30 to 0.50. Comparison with the results of Orton et al. (1992) and Kostiuk et al. (1992) is not straightforward, but Yelle et al. concluded that their ethane densities were consistent with the mixing ratios derived from the infrared data near 0.1 mbar. The C_2H_4 abundance near 300 km was estimated to be roughly a factor of 2×10^{-3} smaller than the ethane abundance; this may be an upper limit. An upper limit of $\sim 1.5 \times 10^{-7}$ for the C_2H_2 mixing ratio near 0.1 mbar was also derived. Comparison with the infrared-derived results is again not straightforward but consistency is indicated.

D. Evidence for Latitudinal and Temporal Variations

The clearest evidence for spatial and temporal variations comes from observations of cloud and haze layers in the Neptune atmosphere (see the Chapter by Baines et al.). There is a substantial history of groundbased observa-

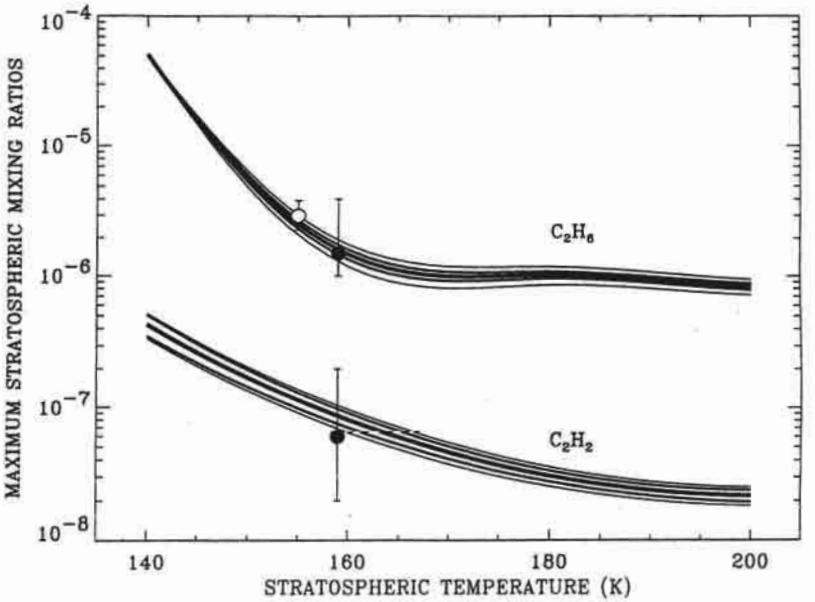

Figure 12. Maximum stratospheric mixing ratios of C_2H_2 and C_2H_6 from the mid-infrared spectral modeling of Orton et al. (1992). Fitted results are shown by the thick central curves; surrounding curves indicate the uncertainty associated with the fitting procedure (inner envelope) and the combined uncertainty of the fit and the absolute calibration (outer envelope). Values for the maximum mixing ratios of C_2H_2 and C_2H_6 derived by Bézard et al. (1991) and associated uncertainties are also shown for their 159 K stratospheric temperature. The open circle and associated 30% uncertainty represents the mixing ratio determined by Kostiuk et al. (1990), plotted at the peak temperature of their "nominal" profile.

tions of temporal variations, while observations of spatial variability have been made possible by recent technical advances and the Voyager flyby. The anti-correlation between Neptune's visible albedo and the solar cycle (Lockwood and Thompson 1991) may be of particular significance as regards the stratosphere, in that the albedo variations may be due to the "tanning" of stratospheric hydrocarbon aerosols by solar ultraviolet photons as proposed by Pollack et al. (1987) to account for the darkness of Uranian stratospheric aerosols. Neptunian hydrocarbon aerosols are more abundant and larger; consequently their shorter sedimentation times should result in the aerosol column manifesting the effects of recent levels of ultraviolet exposure (Baines and Smith 1990). Variations in stratospheric haze layers may also indicate variations in the thermal structure near the condensation levels, which in turn might be driven by the aerosols themselves. Further discussion is to be found in the Chapter by Baines et al.

Data pertaining to variations in the vapor phase abundances of stratospheric hydrocarbons is sparse. Relatively high spatial resolution spectra

obtained by IRIS were investigated by Bézard et al. (1991) for spatial variations in the C_2H_2 emission between 30°N and 80°S. A broad maximum in the zonal mean C_2H_2 emission near the equator and the suggestion of a maximum at the south pole is evident in the resultant averaged spectrum, as is a fairly well-defined minimum near 50 to 60°S (Fig. 13). This latitudinal contrast can be explained by a decrease of 15 K in the mean temperature at 0.03 to 2.0 mbar, a factor of 5 decrease in the C_2H_2 abundance at these pressures, or a combination of both. This meridional variation is similar to that observed at longer wavelengths by the IRIS experiment in the troposphere and lower stratosphere. Whether due to C_2H_2 abundance or temperature variations, Bézard et al. (1991) concluded that the meridional variation was the result of dynamical influences. The observations are consistent with a planetary circulation pattern with upwelling at mid-latitudes and subsidence at low and high latitudes (Conrath et al. 1991*b*), and suggest that this circulation pattern extends at least 200 km above the tropopause. However, Bézard et al. also note that a latitudinal variation in the eddy mixing coefficient in the lower stratosphere driven by small-scale mixing processes could also be responsible.

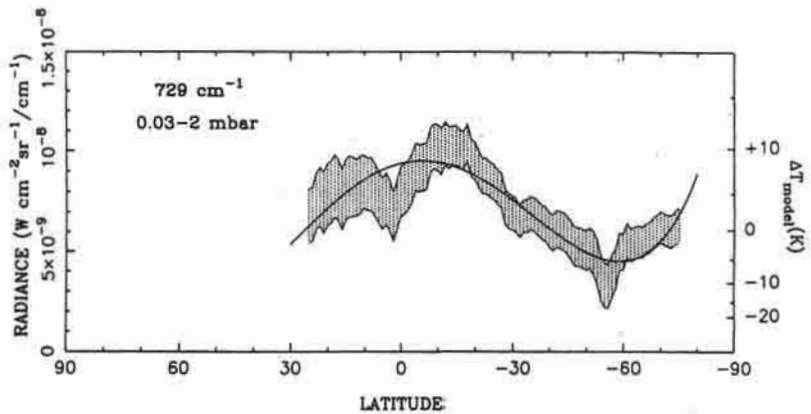

Figure 13. Latitudinal variation of Neptune's radiance at 729 cm^{-1} from Voyager IRIS measurements (Bézard et al. 1991). Spectral radiances measured with relatively high spatial resolution (2280 in number) have been adjusted to normal viewing conditions and fitted with a polynomial (solid curve). The shaded area is the ± 1-σ uncertainty zone obtained from a separate binning procedure. The right-hand ordinate axis indicates the temperature excursion from a mean stratospheric temperature of 159 K implied by the left-hand axis radiance levels for a fixed C_2H_2 mixing ratio of 6×10^{-8} (CHES profile).

A secular increase in the disk-averaged 12 μm C_2H_6 emission from Neptune was suggested by Orton et al. (1987) after comparing their results with those of Gillett and Rieke (1977), who also had noted a similar difference between two of their data sets taken some two years apart. Using similar moderate resolution (~2%) spectral observations, Hammel et al. (1992) re-

ported a statistically significant increase in the ratio of the C_2H_6 and CH_4 emissions compared with the Orton et al. (1990) spectrum. The consistency of their CH_4 emission measurements in 1989 and 1991 with the Orton et al. (1990) spectrum suggests that the globally averaged CH_4 mixing ratio and mean stratospheric temperature were roughly stable over the 6 yr time span between the observations; unfortunately, the Gillett and Rieke noise level was too high to extend this comparison back to 1975. Hammel et al. (1992) tentatively attributed the observed change to an increase of 15% or more in the C_2H_6 abundance. If further observations verify a significantly larger change in the C_2H_6 emission compared with the (somewhat noisier) CH_4 emission, a case can be made for real secular changes of the C_2H_6 abundance.

E. HCN and CO in the Stratosphere

Observations at submillimeter wavelengths have identified HCN in the stratosphere and CO in the stratosphere and tropcsphere of Neptune; simultaneous measurements have failed to detect the presence of these species on Uranus. The mixing ratios of HCN and CO in the stratosphere are 1.2×10^{-9} and 1.2×10^{-6}, respectively, from observations carried out with the James Clerk Maxwell Telescope and the Caltech Submillimeter Observatory (Marten et al. 1991,1993); the CO tropospheric mixing ratio is similar to the stratospheric value (Guilloteau et al. 1993). Observations carried out with the telescope at the Institut de Radio Astronomie Millimetrique yielded similar (but somewhat lower) mixing ratios in the stratosphere (Rosenqvist et al. 1992): $6.5(\pm 3.5) \times 10^{-7}$ for CO and $3.0(\pm 1.5) \times 10^{-10}$ for HCN, along with upper limit mixing ratios of 4×10^{-10} for HC_3N and 5×10^{-9} for CH_3CN. The differences between the JCMT-CSO and IRAM HCN abundance determinations have recently been discussed by Lellouch et al. (1994). The discovery of HCN and CO was particularly surprising, as the conventional wisdom had held that all nitrogen in Neptune's atmosphere was bound up chemically in NH_3 and segregated almost exclusively in the troposphere, and that CO must have been converted to CH_4. Modeling of the HCN abundance has been controversial. The dispute pivots on the source for the observed HCN: an "intrinsic" source from dissociation of N_2 transported upward from the troposphere, or an "external" source involving an N or N^+ flux onto the top of Neptune's atmosphere from Triton. (For further discussion, refer to Sec. IV.E below and to the Chapter by Gautier et al.).

IV. MIDDLE ATMOSPHERE MODELING

In order to reconcile and understand the numerous observational results on thermal structure, composition, and aerosol distributions collected over the last two decades, it is necessary to resort to modeling. As yet, modeling capabilities have not developed to the point of being able to predict the diverse assemblage of observations reviewed in the previous sections and in the Chapters by Baines et al. and Gautier et al. If and when such capabilities

do emerge, we will be able to rely upon modeling to investigate phenomena not directly observable from Earth. In turn, modeling results can be useful for making comparisons between Neptune and the other outer planets, in attempts to reconstruct the history of the planet and to gain clues as to its formation, and (hopefully) to help define mission requirements for a return to Neptune.

Outstanding current issues to be addressed by modeling are: (1) explaining the observed thermal structure and reconciling this structure with radiative-convective models; (2) explaining the apparent abundance of methane in the stratosphere in excess of cold-trap saturation values; (3) reconciling observed vapor phase abundances of hydrocarbons with measurements pertaining to stratospheric aerosols; (4) reconciling the strength of and vertical variation in eddy mixing implied by observed hydrocarbon abundances with dynamical models; and (5) unraveling the implications of the recent observations of HCN and CO in the stratosphere. Aerosol observations and modeling related to topic 3 are discussed in the Chapter by Baines et al.

A. Modeling of the Middle Atmosphere Thermal Structure

The earliest work on modeling radiative and convective equilibrium processes in Neptune's atmosphere was done by Trafton (1967), who established that the collision-induced dipole transition of H_2 was responsible for most of the infrared opacity. However, his models omitted CH_4 as an agent of radiative heating and cooling in the stratosphere; thus, his models lacked the characteristic "temperature inversion" in the lower stratosphere seen in Fig. 1. Macy and Trafton (1975) explored models with arbitrary solar energy deposition functions, similar to those of Danielson (1977) and Danielson et al. (1977) for Uranus. An early attempt to determine the stratospheric temperature structure from a mathematical "inversion" of the 7.8 μm emission spectrum was carried out by Courtin et al. (1979) who decided that a uniform CH_4 mixing ratio on the order of 2×10^{-3} fitted the available data most successfully. This value exceeds the local saturation mixing ratio throughout much of the lower stratosphere; its vertical uniformity requires extremely vigorous vertical mixing in the lower stratosphere and is considered unrealistic.

Later work by Appleby (1986) on one-dimensional radiative-convective modeling incorporated constraints on the thermal structure obtained from more recent thermal infrared and stellar occultation observations. He also modeled CH_4 radiative heating and cooling in the near-infrared using physical models rather than arbitrary functions. Temperatures at $p \lesssim 0.1$ mbar inferred from stellar occultations were attained only in models with significant direct heating from absorption of solar radiation. His preferred model (model "e", Fig. 1) is characterized by a CHES distribution for methane with $f_S(CH_4) = 0.02$ and a uniformly distributed stratospheric aerosol burden; however, he noted that his preference for this "convective penetration" model (Sec. IV.B) was due in part to a lack of independent evidence for relatively high heating rates from aerosol absorption above the troposphere. In fact, however, his model "c" (Fig. 1), characterized by localized aerosol heating near 1 mbar,

exhibits larger temperatures for $p<1$ mbar than model "e". While this particular model was not consistent with all the infrared data available to Appleby, with hindsight it suggests that aerosols in the lower stratosphere may play a significant role in establishing the observed $p-T$ structure (Baines and Smith 1990).

Using a time-dependent model, Bézard (1989) calculated the seasonal variations in atmospheric thermal structure expected for Neptune under radiative-convective equilibrium conditions, i.e., ignoring meridional heat transport. For the epoch of the Voyager encounter with Neptune, just before northern winter solstice, his models predicted that the north polar region should be warmer than the south by ~3 K at the tropopause (p = 100 mbar) and the south polar region warmer than the north by ~12 K near 0.3 to 1 mbar as a result of the different time scales in radiative response in the stratosphere vs troposphere. Conrath et al. (1990) presented a series of time-dependent linear radiative-dynamical model results for meridional stratospheric circulations on Jupiter, Saturn and Uranus; while this model contained neither an accurate representation of the detailed radiative heating and cooling nor dynamical forcings within the modeled pressure regime, it was useful in illustrating the potential influence of dynamics. Conrath et al. (1991*b*) subsequently applied this model to the IRIS results from the Neptune encounter. Observed zonal wind speeds from cloud top motions were used to specify the lower boundary condition. The modeled temperatures were generally cooler than observed values, suggesting a greater solar energy deposition rate in the stratosphere than modeled from gaseous absorption alone. Nevertheless, Conrath et al. (1991*b*) were able to reproduce the correct equator to midlatitude temperature gradient for a Rayleigh friction time constant of the same order of magnitude as the radiative relaxation time constant, in line with the modeling results of Conrath et al. (1990) for the other giant planets.

Appleby (1990) has recently studied the effects of CH_4 vibrational relaxation in radiative equilibrium models of the upper stratospheres of the giant planets and has shown that non-LTE effects can be appreciable for $p \lesssim 0.01$ mbar. Although the upper stratosphere is far from LTE (local thermodynamic equilibrium) in his models for Neptune, the nominal thermal structures are not significantly different from LTE profiles like those shown in Fig. 1. This is attributed to a "fortuitous" grouping of CH_4 vibrational states giving rise to non-LTE heating and cooling rates that are closely related and differ by multiplicative factors of order unity. To illustrate the possible consequences of uncertainties in collisional relaxation rates, "extreme" non-LTE models were explored; these suggest that departures from LTE models as large as ± 20 K at 0.1 μbar are possible. Comparisons with stellar occultation $p-T$ profiles led Appleby to acknowledge that localized aerosol heating or dynamical processes may be needed to explain the complex features exhibited by these profiles; nevertheless, the non-LTE character of the upper stratosphere should not be ignored when modeling nonradiative forcings.

The current state of knowledge of Neptune's stratospheric temperature

and composition creates a problem for radiative equilibrium models. For example, work presented by Friedson and Orton (1992) supports the conclusion of Appleby (1986) that, unless $f_S(CH_4)$ is near the 1% level, there is insufficient radiative heating of the atmosphere to support the warm temperatures observed. This conclusion, however, must be re-examined in the light of the most recent efforts to derive the properties of stratospheric aerosols (see the Chapter by Baines et al.); Baines and Smith (1990) have estimated that 6 to 14% of the solar flux at visible wavelengths is absorbed by stratospheric aerosols at pressures 2 to 20 mbar. Additional nonradiative heating mechanisms may also be operative. It has been suggested (Wang and Yelle 1992; Wang 1993) that the source(s) (as yet unidentified) providing the energy needed to explain the observed thermospheric temperature profile can, via conduction, heat the stratosphere at pressures $\lesssim 1$ μbar to temperatures of $\sim$150 K.

The dissipation of vertically propagating inertia-gravity waves is another potential heating mechanism. Roques et al. (1994) have most recently advocated this hypothesis, on the basis of simple estimates of heating rates inferred from wave-like features in the $p-T$ profiles derived from their stellar occultation lightcurves (Sec. II.B). However, these profiles are increasingly suspect for pressures smaller than 1 μbar, and the arbitrary criterion by which they have selected their preferred $p-T$ profiles may have biased their estimates. They also note that the apparent solar cycle variation in mean stratospheric temperatures unveiled in their analysis may be tied to variations in aerosol abundances in the stratosphere (Lockwood and Thompson 1991).

B. Transport of CH_4 into the Stratosphere

So far, the weight of evidence points to a global average mixing ratio of CH_4 in the stratosphere of Neptune larger than is consistent with the operation of a simple tropopause cold trap; if the simple cold trap worked, then the stratospheric mixing ratio would be established by vapor phase saturation of the species in question at the pressure and temperature of the tropopause. The only plausible source of stratospheric methane is upward transport from the troposphere, where $f(CH_4) \approx 0.02$ at levels below the apparent methane haze layer at 1.7 bar (see the Chapters by Gautier et al. and by Baines et al.). As described earlier, there is still uncertainty surrounding the actual mixing ratio of methane in the stratosphere ($10^{-4} \lesssim f_S(CH_4) \lesssim 10^{-3}$), and there is sufficient variation in tropopause temperatures (Fig. 4 of the Gautier et al. Chapter) that an exact value for the cold trap mixing ratio cannot be specified ($10^{-5} \lesssim f_{TRAP}(CH_4) \lesssim 10^{-4}$). Nevertheless, it seems likely that $f_S(CH_4)$ exceeds $f_{TRAP}(CH_4)$ by a factor approaching 10 (Bishop et al. 1992; Yelle et al. 1993), so we need to explain why.

Hunten (1974) briefly mentioned the ideas of a "leaky" cold trap and the lofting of small particles directly into the stratosphere by strong tropopause-penetrating updrafts. Macy and Trafton (1975) discussed the inference that $f_S(CH_4) > f_{TRAP}(CH_4)$ in the Neptune stratosphere from infrared data demon-

strating the existence of the temperature inversion and cited Hunten's ideas as perhaps helping to explain the situation. Appleby (1986), in his comprehensive radiative-convective modeling of infrared data available at the time, came down in favor of $f_S(CH_4) > f_{TRAP}(CH_4)$ and gave the mechanism for maintaining this situation a name: "convective penetration." He described two basic scenarios. In the vapor mode, actual supersaturations in the vicinity of the tropopause could exist if there was a lack of condensation nuclei or if upward transport was too rapid for condensation to occur before the gas was swept into warmer regions. If this vapor phase penetration occurred at well-separated, localized sites (as seems to be required by the evidence for a stagnant lower stratosphere, at least on global scales), then condensation equilibrium would continue to hold in a global average. The analysis of Moses et al. (1992) on the difficulty of initiating nucleation under stratospheric conditions at Neptune is illuminating in this regard, but inasmuch as the potential convective motions must originate in the upper troposphere where a methane haze already exists, the envisioned convective motions must also carry aloft haze particles which would act as sites for further condensation as the temperature drops. This leads to Appleby's second scenario, the entrainment of haze particles and their "deposition" at lower pressures above the tropopause where temperatures are warm enough to cause sublimation.

Lunine and Hunten (1989) and Stoker and Toon (1989) have carried out more explicit studies of the convective penetration mechanism, using the one-dimensional steady-state entraining jet model of Stoker (1986). These are pre-Voyager studies and both were concerned with explaining the breakdown of cold trapping at the tropopause leading to $f_S(CH_4) = 0.02$ in terms of "buoyant moist convection." Lunine and Hunten (1989), the earlier of the two studies, argued that either CH_4 was moderately supersaturated at the base of the troposphere haze layer or else it was necessary to invoke vigorous dynamics within this haze layer over much of the planet to lift CH_4-bearing parcels above the nominal base of the haze layer a significant fraction of a scale height. Given the arguments of Moses et al. (1992), the supersaturation at the base of the haze layer may be plausible. However, Lunine and Hunten also relied on a large K ($\gtrsim 10^5$ cm^2 s^{-1}) in the lower stratosphere which is hard to justify. Stoker and Toon (1989) criticized Lunine and Hunten for relying on the presence of a methane haze layer thicker than consistent with observations, and argued that moist convection initiated by the buoyancy of drier gas was more plausible. It would be very interesting to see revised work along these lines, incorporating the knowledge gained in the Voyager encounter (e.g., the locations and optical depths of haze layers in the upper troposphere and lower stratosphere and the upper tropospheric lapse rate), particularly because it is no longer believed that $f_S(CH_4)$ can be as large as 2%.

C. Photochemical Modeling of Hydrocarbons

The stratosphere of Neptune is photochemically very similar to Uranus. On

both planets only one photochemically active parent species, methane (CH_4), survives the cold trap at the tropopause in sufficient abundance to be important. Other photochemically active species believed to be present in the troposphere, e.g., hydrogen sulfide (H_2S), ammonia (NH_3), and phosphine (PH_3), are removed from the vapor phase by condensation into various clouds well below the tropopause (see the Chapters by Gautier et al. and by Baines et al.). A quantitative understanding of the chemistry driven by methane photolysis is important for the modeling of stratospheric hazes on Neptune. Methane transported from the troposphere into the stratosphere is converted to C_2 and higher order organics by photolysis and subsequent chemistry. Unit optical depth for Lyman α absorption by methane, $\tau_{CH_4}(\mathrm{Ly}\alpha) = 1$, which defines the primary photolysis level, occurs at pressures $\lesssim 1.0\,\mu$bar. The subsequent mixing of stable photolysis products to deeper pressure levels ($\sim$10 mbar) leads to the formation of hazes, because several of these products (e.g., C_2H_2, C_2H_6, C_3H_8) condense at the pressures and temperatures characterizing the lower stratosphere. Thus, in a steady state situation, the photolytic destruction of methane determines the haze production rate.

To date, two detailed models of methane photochemistry on Neptune have been advanced that address haze formation and production, described in depth in Moses (1991) and Romani et al. (1993). Both are one-dimensional steady-state models. These models divide the atmosphere into a number of horizontally uniform layers and solve the coupled continuity equations for the abundances (or volume mixing ratios) of methane and its photolysis products at each level:

$$\frac{\mathrm{d}F_i}{\mathrm{d}z} = P_i - L_i \tag{1}$$

where z is the altitude, F_i is the flux of species i in units of molecules cm^{-2} s^{-1}, and P_i and L_i are the chemical production and loss rates in units of molecules cm^{-3} s^{-1}. The expression for the flux is

$$F_i = -N(D_i + K)\frac{\mathrm{d}f_i}{\mathrm{d}z} - D_i N f_i \left(\frac{1}{H_i} - \frac{1}{H}\right) \tag{2}$$

where N is the atmospheric number density, D_i is the molecular diffusion coefficient of the ith species with respect to the background atmosphere, K is the eddy mixing coefficient, f_i is the mixing ratio of the ith species, H_i is the species scale height, and H is the atmospheric scale height. The nominal region of interest extends from the tropopause to an upper boundary placed at least a scale height above the methane homopause. The main region of interest, especially for C_2 species, lies between the $\tau_{CH_4}(\mathrm{Ly}\alpha) \approx 0.1$ level and the bottom of the condensation zone: 30 mbar$\gtrsim p \gtrsim$0.1 μbar. The atmosphere is well-mixed at these pressures. It is only at altitudes above the primary photolysis level approaching the homopause that molecular diffusion begins to play a role. All of the dynamics is in effect buried in the parameter K, the magnitude of which is representative of the strength of vertical mixing

in the atmosphere driven by whatever source (e.g., turbulence, meridional circulation) (Sec. IV.D). Consequently, the calculated mixing ratios f_i are usually viewed as being averaged over latitude and longitude but the extent of the averaging region is ill defined. If the chemical lifetime of a species is much shorter than the transport time (roughly H^2/K), then the flux term in Eq. (1) can be neglected and the mixing ratio obtained by equating chemical production to loss at each level. Otherwise, the full set of continuity equations must be solved numerically. Figure 14 presents a simplified schematic of the photochemical system that occurs following the photolysis of methane; other discussions of the chemical pathways arising in the stratospheres of the outer planets can be found in Yung et al. (1984), Strobel (1985), and Atreya (1986).

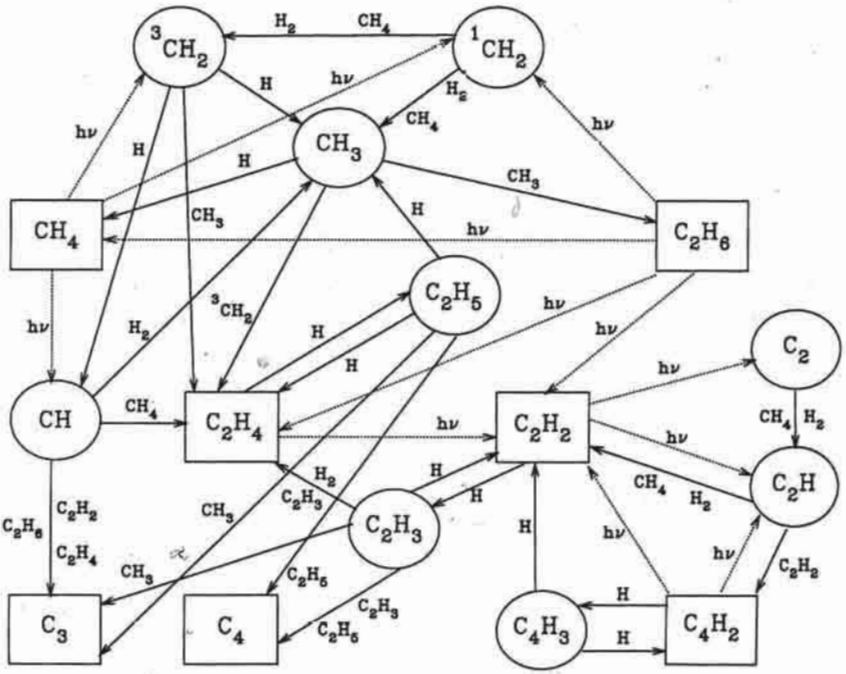

Figure 14. Diagram of the major photochemical pathways following methane photolysis in the model of Romani et al. (1993). Solid lines represent chemical reactions while dashed lines are photolysis pathways. Species in boxes are stable chemical compounds, those in ovals are free radicals.

Models of this type can be used to explore our understanding of methane photochemistry and eddy mixing in the Neptune stratosphere by making careful comparisons to relevant observations. If the chemical pathways and reaction rates are known exactly, then the eddy mixing coefficient can be treated as a free parameter to be varied until the model results are in agreement with the observations. The basic modeling inputs are (hopefully) constrained

by observations: the incident photolysing EUV+FUV photon flux, the model atmosphere, and the rate of supply of methane from the upper troposphere. The incident photon flux is well characterized, the principal component being the direct solar flux. At Neptune's distance from the Sun, however, the pervasive Lyman α skyglow associated with the local interstellar medium (LISM) is not negligible (Strobel et al. 1990); the estimated contribution to the CH_4 photolysis rate is $\sim 3 \times 10^{-9} s^{-1}$ based on near-encounter LISM measurements by the Voyager UVS. However, there are uncertainties in the stratospheric $p - T$ structure (Sec. II.D) and in the value of the methane mixing ratio in the lower stratosphere (Sec. III.B). Also, the photochemical models incorporate a number of photoabsorption cross sections, quantum yields, and reaction rate coefficients which either have not been measured or must be estimated from measurements made at high temperature and/or pressure. What can be done in a modeling study is to determine the model sensitivities to these limitations. With respect to the photochemistry it is important to keep in mind that not all reactions are of equal importance; a model can be very sensitive to one reaction rate while insensitive to another. The determination of model sensitivities to reaction rates, variations in the K profile, etc., points the way to future work.

The models described in Moses (1991) and Romani et al. (1993) differ in their photochemical schemes, in their treatment of vertical transport, and in their analysis of haze formation and production. Detailed discussion of chemical pathways, rate coefficients, etc., can be found in Moses (1991) and Romani et al. (1993) and references cited therein. The main differences in the photochemical schemes and in the handling of vertical transport will be discussed first, in terms of comparisons of the modeling results to the ethane and acetylene mixing ratios retrieved from groundbased and Voyager infrared observations. The global average abundances of C_2H_2 and C_2H_6 in the vapor phase near the 0.2 mbar level are reasonably well established, as discussed in Sec. III.C, with values 6×10^{-8} and 1.5×10^{-6}, respectively, for a mean temperature of 160 K.

The photochemical reaction scheme of Moses (1991) is more extensive than that of Romani et al. (1993) in that it includes a reasonably complete suite of photolysis and reaction pathways for C_3 and C_4 compounds; appreciable steady state abundances of methylacetylene (CH_3C_2H) and propane (C_3H_8) are predicted by their model (Fig. 15). The Romani et al. scheme is complete through the C_2 compounds, but, for the C_3 and C_4 species, it includes only the pathways to production. Nevertheless, Moses (1991) (updated in Moses et al. 1992) and Romani et al. (1993) reached similar conclusions on several points in trying to reproduce observed hydrocarbon abundances. They agree that ethane is the dominant end product from methane photolysis on Neptune. In the Moses et al. (1992) model this species accounts for 84% of the total return flux of carbon atoms to the troposphere (in the form of settling haze particles) while in Romani et al. (1993) it accounts for 70% of the total downward flux. They agree in the inference of a sluggish lower stratosphere ($K \lesssim 10^4$ cm^2 s^{-1}

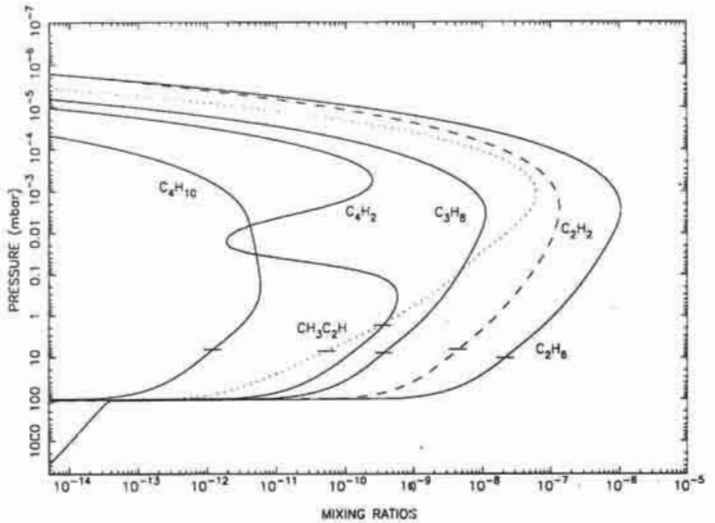

Figure 15. Photochemical model abundances for several stable product hydrocarbons expected to condense in the lower stratosphere, from Moses et al. (1992). Calculations are for Voyager ingress conditions, solar maximum FUV+EUV fluxes (including the LISM source), a CH_4 mixing ratio at the lower boundary of 2×10^{-4}, and a conventional K profile (Eq. 4) with $\beta = 0.66$ and a value of 10^8 cm^2 s^{-1} at the methane homopause; condensation losses were not included in the model. The crossmarks on these profiles indicate the pressures at which these species become saturated.

for $p \gtrsim 10$ mbar). They also concur that the model results are not very sensitive to the CH_4 mixing ratio in lower stratosphere because methane photolysis at Neptune is a photon-limited process. Romani et al. noted that with similar solar FUV+EUV fluxes, model atmosphere, and K profile, C_2H_2 and C_2H_6 mixing ratios from the two models agreed to within an average of 35% in the 1.0 to 0.1 mbar region (above the condensation regions of these species).

Vapor phase hydrocarbon abundances predicted by the models in the pressure region sounded by infrared measurements (~0.1 mbar) are very sensitive to the local value of K. In this region ethane is flowing downward from a production region at higher altitudes (~1 μbar) to a condensation sink at lower altitudes (~10 mbar). Ethane is photochemically stable in this region, i.e., its photochemical lifetime is much longer than the transport time, so transport governs the vertical distribution. Continuity then requires a balance between the overhead net column chemical production rate and the local downward flux. To first order, the downward transport speed is K/H and the mixing ratio for species i is inversely dependent upon K:

$$f_i(z) = \frac{\mathcal{P}_i(z)H(z)}{N(z)K(z)} + C \tag{3}$$

where $\mathcal{P}_i(z)$ is the column-summed net photochemical production rate above altitude z, C is an integration constant and the other quantities have already

been defined. The situation is more complicated for acetylene, which is photochemically active in this pressure region; nonetheless, similar considerations apply (Romani et al. 1993).

Both Moses (1991) and Romani et al. (1993) agree that K profiles of the type

$$K = K_\circ \left(\frac{N_\circ}{N}\right)^\beta \tag{4}$$

(where $K_\circ$ and $N_\circ$ are the eddy mixing coefficient and number density at a reference level and $\beta \approx 1/2$) do a poor job of reproducing simultaneously the observed C_2H_2 and C_2H_6 abundances, although it is possible to adjust this type of K profile to reproduce either the observed C_2H_2 or C_2H_6 abundance alone (Bézard et al. 1991). Moses (1991) did not explore other types of K profiles. In the Moses et al. (1992) model the vapor phase ethane abundance is on the order of 10^{-7} at 1.0 to 0.1 mbar (Fig. 15), too low compared with the value from the infrared observations, while the model acetylene abundance is in reasonable agreement with the infrared observations. Romani et al. (1993), however, experimented with the form of K and were able to fit the IRIS observations with K profiles having relatively low values in the lower stratosphere ($K \approx 2 \times 10^3$ cm^2 s^{-1} for $p \gtrsim 2$ mbar) and relatively high values in the upper stratosphere ($K \gtrsim 5 \times 10^7$ cm^2 s^{-1} for $p \lesssim 0.5$ mbar), with a rapid transition at intermediate pressures, i.e., a rapidly mixed upper stratosphere overlying a stagnant lower stratosphere (Fig. 16). The stagnant layer inhibits the flow of ethane to its condensation sink allowing the mixing ratio to build up, while the region of vigorous mixing at higher altitudes enhances the conversion of C_2H_4 to C_2H_6 which otherwise would be photolysized to C_2H_2. The value of K in the stagnant region was suggested by the inferred overturning time of the lower stratosphere from the circulation pattern presented in Conrath et al. (1991*b*).

Regarding the handling of condensation, Moses et al. (1992) did not include condensation losses in their photochemical model. Instead their photochemical model was used to predict vapor phase hydrocarbon abundances which in turn were used to estimate the supersaturations in the lower stratosphere needed to initiate condensation via homogeneous, heterogeneous, and ion-induced nucleation. Moses et al. concluded that unless condensation to the available nuclei is very efficient, supersaturations on the order of 20 for C_2H_2 and C_2H_6 are required to initiate nucleation. The Romani et al. (1993) models assume that the initial formation of condensation nuclei has already taken place, and include a condensation loss scheme based upon diffusive loss of the vapor phase molecules to pre-existing ice spheres. Romani et al. found that once ice crystals are present they can give rise to rapid loss of vapor phase molecules, reducing the supersaturations to near unity. Nucleation on inefficient condensation nuclei can take place simultaneously with diffusive loss of the vapor if the sticking efficiency of the vapor phase molecules to the ice crystals is $\lesssim 0.01$ or if there are very few crystals at the levels where conden-

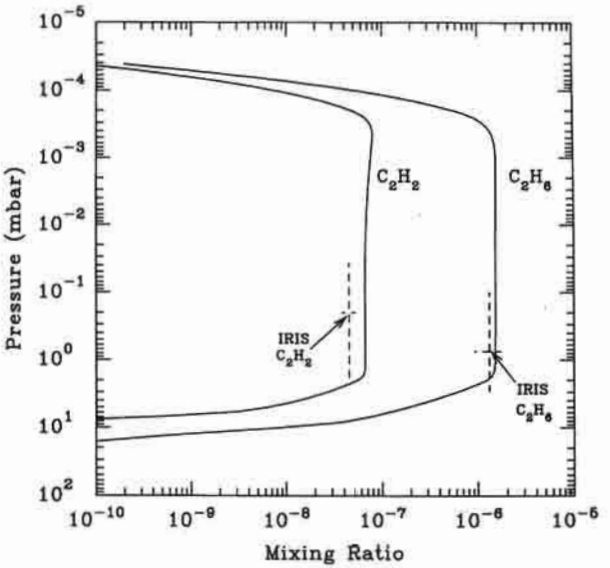

Figure 16. Photochemical model profiles for C_2H_6 and C_2H_2 from Romani et al. (1993; adapted from their Fig. 3), for an eddy mixing profile with $K \approx 2 \times 10^3$ cm^2 s^{-1} for $p \gtrsim 2$ mbar and $K \gtrsim 5 \times 10^7$ cm^2 s^{-1} for $p \lesssim 0.5$ mbar. Calculations are for their nominal egress model atmosphere, solar maximum FUV+EUV fluxes (including the LISM source), a CH_4 mixing ratio at the lower boundary of 10^{-4}, and global average conditions. Vertical dashed lines show IRIS retrieved values of C_2H_6 (1.3×10^{-6}) and C_2H_2 (4.5×10^{-8}) and the region of IRIS sensitivity for this model atmosphere with CHES profiles (full widths at half maximum of the contribution functions). Horizontal dashed lines indicate the measurement uncertainties in the IRIS-retrieved mixing ratios and are located at the peak of the contribution function.

sation first takes place (i.e., where the majority of the diffusive loss occurs). Alternatively, nucleation and ice haze formation in Neptune's stratosphere may be episodic.

Constraints on the total amount of condensable hydrocarbons produced in a model are provided by comparing predicted haze production rates with available stratospheric haze observations (described in the Chapter by Baines et al.). Moses et al. predicted an ice haze production rate of 2.2×10^{-15}g cm^{-2} while Romani et al. predicted 1.0×10^{-14}g cm^{-2}. Using these rates we can estimate corresponding column densities for haze particles by balancing production with sedimentation loss for particles of a given size. Pryor et al. (1992), from analysis of the Voyager PPS data, retrieved a stratospheric haze column density of 2.5 to 6.2×10^7 particles cm^{-2} in the 20° to 30°S latitude band with a mean particle radius of 0.20 to 0.25 μm. Baines and Hammel (1994), from multi-spectral analysis of groundbased observations of Neptune, have deduced a global average column density of 6.4×10^7cm^{-2}, assuming 0.2 μm radius particles, similar to the Pryor et al. results. Using the PPS upper limit on particle size the Romani et al. results correspond to a column density

of $7.7 \times 10^7 cm^{-2}$, 24% larger than the PPS maximum value, while the Moses et al. model yields $4.3 \times 10^7 cm^{-2}$ for 0.2 μm radius particles, within the PPS range. Solar maximum FUV+EUV fluxes were used by both Moses et al. and Romani et al. Romani et al. argued that owing to weak eddy mixing in the haze formation region, haze production rates should be averaged over a solar cycle; making that adjustment, their model is then in agreement with the PPS observations for particle radii in the range 0.22 to 0.25 μm. The PPS data also indicate that most of the haze lies at pressures >5 mbar, which both models predict.

In Romani et al. (1993), photochemical models generated to fit the groundbased and Voyager infrared data were also tested against the UVS solar occultation lightcurves. The lightcurves at wavelengths longward of 153 nm place stringent constraints on the abundance of C_2H_4 in the upper stratosphere. It was evident in these comparisons that the photochemical models exhibited larger ethylene abundances than were consistent with the UVS data unless there was a region of enhanced K near 10 μbar in the modeling. Ethylene is primarily produced by $CH_4 + CH \rightarrow C_2H_4 + H$ near 1.0 μbar but the main loss channel is $H + C_2H_4 + M \rightarrow C_2H_5 + M$ that occurs efficiently only at deeper levels. A zone of rapid mixing near 10 μbar with weaker mixing at $p<1.0$ μbar will transport ethylene downward to where the three-body association reaction proceeds quickly. This not only reduces C_2H_4 model abundances, but also boosts the production of ethane in that the principal fate of C_2H_5 is $C_2H_5 + H \rightarrow 2CH_3$ followed by $CH_3 + CH_3 + M \rightarrow C_2H_6 + M$. This inference that K reaches a localized maximum near 10 μbar is fairly independent of uncertainties in the chemical reaction rates adopted in Romani et al. (1993), because its requirement essentially stems from the displacement of the C_2H_4 loss zone from the production zone. More detailed modeling of the UVS solar occultation lightcurves is currently being carried out.

Recently Mordaunt et al. (1993) have determined that CH_3 is produced with a quantum yield of ~0.5 in methane photolysis at Lyman α. Prior work (see, e.g., Slanger and Black 1982) had indicated that the major C-radical generated in the photolysis was methylene ($^{1,3}CH_2$). At first glance this would seem to be a major perturbation to the chemistry in Moses et al. (1992) and Romani et al. (1993). However, in these models the $^1CH_2$ quantum yield at Lyman α is ~0.5; once formed, $^1CH_2$ reacts rapidly with H_2 to form CH_3. Thus the models already have the production of CH_3 from CH_4 photolysis at nearly the right quantum yield. What is important, and was not well determined by Mordaunt et al. (1993), is the net quantum yield for production of CH_3 and $^1CH_2$ vs CH and $^3CH_2$. The first set of products leads to ethane production (along with methane recycling) while the second set yields C_2H_4 and C_2H_2. Romani et al. noted that to reproduce the abundance ratio $[C_2H_6]/[C_2H_2]$ obtained from IRIS measurements (Bézard et al. 1991), it was necessary to increase the Lightfoot and Pilling (1987) rate coefficient for $H + C_2H_4 + M \rightarrow C_2H_5 + M$ by a factor of two, thereby increasing the fraction of ethylene converted to ethane at the expense of the photolysis path

to acetylene. If further studies of methane photolysis show that the fraction of ethylene precursor formation is too high in the current models, then the need for the doubling of this rate could be relaxed. However, rapid downward transport and subsequent C_2H_4 loss via this reaction will still be needed to satisfy the UVS solar occultation constraints.

D. Eddy Mixing Profiles

To date, several constraints on the strength of eddy mixing in the stratosphere of Neptune have been derived from Voyager measurements. Parkinson et al. (1990) analyzed He 584 Å dayglow measurements from the UVS instrument and derived a K value of $5^{+11}_{-4.4} \times 10^7$ cm^2 s^{-1} nominally referenced to the helium homopause, assuming a 1.0 μbar temperature of 150 K and f(He) = 0.19 in the mixed atmosphere (Sec. V.B). The analysis by Bishop et al. (1992) of the UVS solar occultation lightcurves extracted K values near 0.2 μbar of $\sim$3 to 10×10^6 cm^2 s^{-1} depending on the adopted $p-T$ model and K profile form. Yelle et al. (1993) obtained $K \approx 5 \times 10^6$ cm^2 s^{-1} at 550 km altitude ($p \approx 0.6$ μbar) at the egress latitude, consistent with those egress models of Bishop et al. with either T = 180 K or $f_S(CH_4) > 10^{-3}$. By utilizing C_2H_6 densities obtained from the UVS data at longer wavelengths, Yelle et al. derived $K \approx 10^5$ cm^2 s^{-1} near 30 μbar. The eddy mixing profile adopted in their modeling had K constant at pressures $\gtrsim$40 mbar and exponentially increasing with decreasing pressure, limited to a maximum value of 10^8cm^2 s^{-1} based on the Parkinson et al. estimate.

Observational constraints on K at deeper levels have been inferred from IRIS data, as well as groundbased infrared measurements. Photochemical modeling of the Bézard et al. (1991) and Kostiuk et al. (1992) spectra strongly suggests the presence of a stagnant lower stratosphere, as described in Sec. IV.C. Moses (1991) reached a similar conclusion on the basis of her modeling of infrared-derived hydrocarbon abundances. Equation (3) can, in fact, be employed to derive an upper limit to K from the C_2H_6 abundance near 0.5 mbar. Assuming for the moment that each CH_4 Lyman α photoabsorption event results in ethane production, the global average C_2H_6 column production rate would be $\sim 3 \times 10^8$ cm^{-2} s^{-1} and the corresponding upper limit on K near 2.0 mbar is 8×10^3cm^2 s^{-1}. The inference of Yelle et al. that K remains constant at 10^5cm^2 s^{-1} for pressures greater that 0.05 mbar therefore seems inconsistent with these estimates, though a combined analysis of the UVS and infrared data may resolve this. The comparisons of UVS solar occultation lightcurves with simulated lightcurves generated from photochemical models satisfying infrared-derived constraints presented by Romani et al. (1993) are encouraging in this regard; these comparisons also suggest a region of enhanced vertical transport near 10 μbar, as noted in Sec. IV.C.

Owing to the lack of detailed knowledge regarding dynamics and the distributions of minor species in the middle atmospheres of the outer planets, it has been common practice to adopt forms for the variation of K with altitude or pressure developed in (older) terrestrial studies; these are then applied in

photochemical modeling by treating K as a free parameter to be determined by data-model comparisons. To the extent that the remaining physics addressed by one-dimensional photochemical transport codes is correct, a fitted K profile may yield some insight into the dynamical state of the middle atmosphere in question. It is important to recognize, though, that vertical transport can be driven by numerous processes (turbulent mixing, advection) and that the relative significance of these processes is affected by chemistry. The form given by Eq. (4) has been used more often than not (Lindzen 1971; Hunten 1975), with $\beta = 0$ or 1/2; the latter choice was initially justified by reference to transient vertically propagating waves. Both Moses et al. (1992) and Romani et al. (1993) treated K_o and β as fitting parameters in their handling of this form for K.

Lindzen (1981) presented a parameterization of K that addresses the "breaking" of upwardly propagating waves (which occurs when the wave-modified temperature lapse rate exceeds the adiabatic lapse rate, instigating convective instability) in the terrestrial mesosphere; in particular, K increases rapidly in the vicinity of the breaking level. Lindzen was mainly concerned with parameterizing the wave drag acceleration of the mean zonal flow, however, and his parameterization exhibits a strong dependence on the difference between the mean zonal wind speed and the wave phase speed in the zonal direction. This leads to a marked decrease in K at smaller pressures at mid-latitudes, where the deposition of momentum by breaking waves strongly affects upper mesospheric wind speeds; the turbulent mixing generated by waves decreases as the "critical level" (the level where the zonal wind speed approaches the horizontal phase speed of the wave owing to the acceleration stemming from the deposition of wave momentum) is approached. Even for tidal modes in the terrestrial atmosphere (at low latitudes), for which no "critical level" arises, Lindzen argued for a decrease in K at altitudes above the breaking level (and below the nominal homopause), because the rapid increase in molecular diffusion as the homopause is approached will itself act to damp the tide so that less mechanical mixing is needed to adjust for wave-driven convective instabilities.

Holton and Schoeberl (1988) discuss arguments that, as regards the transport of minor constituent species, the Lindzen (1981) parameterization overestimates the magnitude of vertical diffusion caused by breaking gravity waves. The main point of the Holton and Schoeberl paper, however, is to argue that the vertical transport of a minor species in the terrestrial mesosphere is more likely due to advection within a meridional circulation system, unless the species in question is characterized by relatively short photochemical time scales. Notably, the effective one-dimensional vertical transport coefficient they propose, defined in terms of an area-weighted global average of vertical wind speeds obtained in simple numerical simulations, also exhibits a decrease at altitudes above the level where maximum meridional wind speeds occur (i.e., vertical speeds decrease near the top of the meridional circulation pattern).

What is most significant in the context of one-dimensional photochemical models is that the decrease in K exhibited in either scenario occurs at altitudes beneath the nominal homopause, defined as the level above which molecular diffusion is the main process governing vertical transport. These analyses of vertical transport in the terrestrial mesosphere thus offer guidelines that can be tested in the Neptune situation. Namely, we can construct schematic K profiles that exhibit the traits of the K profiles suggested by Lindzen (1981) and Holton and Schoeberl (1988), and rely on data-model comparisons to establish parameter values. This has been the approach followed in the recent photochemical modeling of groundbased and Voyager measurements, examples of which are presented by Romani et al. (1993). In addition to the constraints on K for $p \geq 0.5$ mbar and $p < 1.0\,\mu$bar, the apparent requirement for enhanced eddy mixing at intermediate pressures to bring ethylene abundances into line with UVS constraints is noteworthy.

Models of stratospheric-mesospheric circulations on Neptune have not been developed as yet, so it is not possible to compare photochemically derived K profiles with vertical transport rates associated with expected global or meso-scale wind systems at pressures $\lesssim 1$ mbar. The zonal mean circulation pattern in the lower stratosphere derived from IRIS data by Conrath et al. (1991*b*) suggests sluggish vertical transport, but the $p - T$ profiles upon which this pattern is based only extend up to ~30 mbar. Nevertheless, the overturning rate of the lower stratosphere in this model ($\sim 10^9 s^{-1}$) is consistent with K values required in the photochemical modeling of infrared measurements (Sec. III.C).

Insights into the possible role of upwardly propagating waves in the vertical transport of minor species is available from the Voyager radio occultation data. In a study of wave signatures in the RSS occultation data obtained at Uranus, Hinson and Magalhães (1991) were able to identify two possible vertically propagating wave modes and to derive quantitative estimates for the breaking level and eddy viscosities needed to damp the wave motions using the Lindzen (1981) parameterization. The value of K so obtained was in line with the values suggested by photochemical modeling of the UVS Uranian solar occultation results (Herbert et al. 1987; Summers and Strobel 1989; Bishop et al. 1990), which Hinson and Magalhães took to indicate that wave dissipation was an important source of eddy mixing in the equatorial Uranian stratosphere. A similar analysis of the RSS data acquired at Neptune has revealed distinct atmospheric wave signatures at both ingress and egress locations (Hinson and Magalhães 1993). Two waves, one at each location and identified as most likely being inertio-gravity waves, were modeled to estimate wave contributions to the eddy mixing and momentum budget of the middle atmosphere. Unlike the situation at Uranus, Hinson and Magalhães were able to obtain only upper bounds on the eddy mixing coefficient associated with the two waves; horizontal wavelengths cannot be determined from the RSS data acquired at Neptune, resulting in uncertainty in a number of wave parameters, including K. Based on their modeling, the wave ob-

served at ingress begins to break near 3 mbar and generates eddy mixing at $p<3$ mbar of about $2 \times 10^4 \text{cm}^2\ \text{s}^{-1}$ or less. At pressures $\lesssim 15$ μbar this wave is strongly attenuated by molecular viscosity, so that wave breaking ceases and essentially no eddy mixing is generated at lower pressures. Owing to its larger vertical wavelength, the wave observed at egress should begin to break at a lower pressure, about 0.5 mbar, and the wave-generated eddy mixing at $p<0.5$ mbar could be as large as $50 \times 10^4 \text{cm}^2\ \text{s}^{-1}$. For this wave, damping by molecular viscosity becomes significant at $p \approx 1$ μbar, marking the upper boundary of the region where wave dissipation produces eddy mixing. These upper bounds on K are considerably larger than the results obtained by Hinson and Magalhães for Uranus. Hinson and Magalhães (1993) note that their results are also close enough to other independently derived estimates of K (Bézard et al. 1991; Bishop et al. 1992) to suggest that wave breaking is a significant source of eddy mixing in the middle atmosphere of Neptune. However, as emphasized by Walterscheid and Schubert (1990), the Lindzen parameterization adopted by Hinson and Magalhães for estimating K lacks rigorous justification. Hence, the estimates of K given by Hinson and Magalhães (1991,1993) are rough approximations at best and should be employed with caution.

Wave features in stellar occultation-derived temperature profiles have been alluded to previously (Sec. II.B, Sec. IV.A). These are, in fact, associated with the "spikes" or scintillations that are common features in stellar occultation lightcurves. French and Gierasch (1974), referring to the 1971 β Scorpii occultation by Jupiter, suggested that the thermal perturbations were due to upwardly propagating inertia-gravity waves and that these could contribute significantly to upper stratospheric eddy diffusivities and the overall heat balance. Stellar occultation lightcurve scintillations have also been attributed to density fluctuations associated with turbulence. Simulations of occultation lightcurves by French and Lovelace (1983) explored the relevant assumptions (weak vs strong turbulent scintillation, perfect horizontal layering) and suggested that the numerical inversion of lightcurves in the vicinity of the limb is only weakly influenced by horizontal inhomogeneities in the atmospheric structure. The scintillation phenomenon has been more thoroughly studied by Hubbard et al. (1988) and Narayan and Hubbard (1988) using data from the 20 August 1985 stellar occultation by Neptune (Hubbard et al. 1987). The first of these papers utilized an approximate numerical ray tracing model while the second presented a formal analytic theory; in each case the goal was to analyze the scintillation characteristics arising from variations in atmospheric structure both perpendicular and parallel to the limb so as to address the entire occultation record including the "central flash." The model fits indicate a large aspect ratio for the density fluctuations in Neptune's stratosphere, with a typical horizontal extent (parallel to the limb) a factor of ~ 25 larger than the vertical extent. While confirming the existence of highly anisotropic "turbules," the source of these fluctuations was not addressed. The theory of Narayan and Hubbard assumed a power law

(Kolmogorov) spectrum for the density fluctuations but they noted that the quasi-layered structures causing the scintillations may be due to propagating waves or turbulent layers generated by wave breakdown. Thus, as was also noted by French and Lovelace (1983), careful analysis of stellar occultation data can provide information on both the large-scale vertical structure and the turbulence characteristics of the stratosphere of the occulting planet, which may eventually lead to independent estimates of the strength of eddy mixing and insights into the operative mixing processes.

Neptune is the only outer planet for which it may be possible to construct a complete empirical eddy mixing profile, based on the data acquired during the Voyager encounter. Photochemical modeling of these data using the "conventional" form for K (Eq. 4) has demonstrated that it simply is not appropriate. Eventually, dynamical modeling of outer planet stratospheres may lead to quantitative prescriptions for vertical constituent transport rates driven by turbulence or advection (or both) varying with altitude and latitude; these could then be utilized in two-dimensional photochemical modeling studies that in turn would allow the data on constituent abundances to constrain dynamical modeling. Until then, photochemical modelers should at least recognize the extensive literature on constituent eddy mixing that has been developed in terrestrial studies (see, e.g., Lindzen 1981; Garcia and Solomon 1985; Strobel et al. 1987; Holton and Schoeberl 1988; Dunkerton 1989; Walterscheid and Schubert 1990) and perhaps draw from this body of work guidelines for plausible parameterizations of K. It may also be noted that eddy mixing may transport heat as well as constituents, so that a satisfactory K profile may also shed light on the observed thermal structure.

E. HCN and CO in the Stratosphere

The conventional mechanism for producing HCN on Titan is the reaction between nitrogen atoms and the products of methane photochemistry, particularly CH_3 and to a lesser extent CH_2 (Yung et al. 1984), i.e.,

$$\begin{aligned} N + CH_3 &\rightarrow H_2CN + H \\ H_2CN + (H, N) &\rightarrow HCN + \text{products}. \end{aligned} \tag{5}$$

$$\begin{aligned} N + {}^3CH_2 &\rightarrow CN + H_2 \\ CN + (H_2, CH_4, C_2H_6, C_2H_4) &\rightarrow HCN + \text{products}. \end{aligned} \tag{6}$$

It has been proposed that, within the constraints of available laboratory chemical kinetics data, the same mechanism is responsible for producing HCN in the stratosphere of Neptune (Atreya et al. 1992; Marten et al. 1993; Lellouch et al. 1994), but its viability hinges on the presence of sufficient amounts of N in the stratosphere. The low tropopause temperature of 50 to 55 K effectively prevents the transport of HCN produced in the troposphere into the stratosphere; the saturation HCN mixing ratio at 50 K is a factor of 10^{-20} smaller than the observed stratospheric value. Two scenarios for supplying N to the

stratosphere have been proposed: the supply can be intrinsic to Neptune, in the form of an upward flux of N_2 from the deep troposphere (Atreya et al. 1992; Marten et al. 1993), or it can be in the form of extraplanetary fluxes of N or N^+ onto the top of the atmosphere originating from Triton (Rosenqvist et al. 1992). Lellouch et al. (1994) have recently argued that both sources may be required to account for the observed abundance. Similar considerations do not arise regarding the origin of CO observed in Neptune's stratosphere. Measured tropospheric abundances (Guilloteau et al. 1993) and the fact that CO is not "cold trapped" at the tropopause point conclusively to an intrinsic source.

Richardson et al. (1991) have argued that the Voyager plasma (PLS) experiment determinations of total flux shell heavy ion content in Neptune's magnetosphere indicate that the pickup of magnetospheric ions must be directly from the ionosphere of Triton. The escape rate of nitrogen ions from Triton has been calculated by Yung and Lyons (1990) to be $8 \times 10^{24} s^{-1}$. Assuming all N^+ leaving Triton reaches Neptune, this amounts to an N^+ flux of 10^5 cm^{-2} s^{-1} onto the top of the atmosphere. To produce their observed HCN mixing ratio of 1.2×10^{-9}, however, Marten et al. (1993) require a nitrogen flux into the stratosphere twenty times larger, 2×10^6 cm^{-2} s^{-1}. The disagreement worsens when losses in the magnetosphere (to the solar wind, rings and the moons, and charge exchange with hydrogen) are considered. In another aeronomic model, Summers and Strobel (1991) proposed escape of nitrogen from Triton in the form of neutral atoms, a situation apparently not favored by the PLS observations (Richardson et al. 1991). The escape rate of N atoms from Triton in this model, $3 \times 10^{25} s^{-1}$, translates to an N-atom flux of 2×10^3 cm^{-2} s^{-1} onto Neptune according to Marten et al. (1993), a factor of 1000 too low to yield the observed HCN abundance in their model. Marten et al. (1993) conclude that Triton seems unable to supply the flux of nitrogen to Neptune's stratosphere required by the observations, leaving an internal source of nitrogen (N_2) as the only viable alternative.

The nitrogen flux required by Marten et al. is based in part on the value they adopt for K in the 1.0 mbar region, $10^5 cm^2$ s^{-1}, because HCN is stable in the pressure region sounded by the submillimeter observations and is flowing downward from a production region at higher altitudes to a condensation sink deeper in the atmosphere (cf., Eq. 3). This value of K is consistent with some of the models of Bishop et al. (1992) and with the Yelle et al. (1993) reanalysis of the UVS solar occultation data. Lellouch et al. (1994), however, have recently derived a much lower required extraplanetary nitrogen flux, 7×10^4 cm^{-2} s^{-1}, reflecting their use of a value for K roughly 2 orders of magnitude smaller as advocated by Romani et al. (1993) (Sec. IV.C) and their smaller derived HCN mixing ratio of 3.2×10^{-10} at 2 mbar. Lellouch et al. present photochemical models for both intrinsic and extraplanetary sources of nitrogen and also discuss the implications of N^+ vs N as the form of nitrogen entering the upper atmosphere. While their required flux in the Triton source case is not inconsistent with the Yung and Lyons (1990) and Summers and

Strobel (1991) estimates of total nitrogen escape rates from Triton, Lellouch et al. nevertheless conclude that Triton is unlikely to be the sole source of N for Neptune's stratosphere, given the uncertainties in the efficiency of nitrogen transport from Triton to Neptune.

In addition, a controversy has developed over the nature of the ionizing flux at Triton. The Yung and Lyons (1990) and Summers and Strobel (1991) models took precipitating magnetospheric electrons to be the main ionization source in Triton's upper atmosphere. If ionization is instead mainly due to solar EUV radiation, the major topside ion at Triton should be C^+ (Lyons et al. 1992; Chapter by Strobel and Summers), with an escape rate (thermal) of $\sim 10^{23} s^{-1}$ and an N^+ escape rate an order of magnitude smaller (Lyons et al. 1993). These more recent aeronomic models thus suggest a reduced role for Triton as a source of nitrogen for the Neptune stratosphere, and reinforce the requirement for a significant intrinsic source of nitrogen.

As discussed in Sec. II.A and in the Chapter by Gautier et al., the mixing ratio of N_2 in the upper troposphere and lower stratosphere might be as large as 0.006 (Conrath et al. 1993). Once convected from the interior to the stratosphere, N_2 can undergo dissociation to nitrogen atoms. However, solar EUV photodissociation cannot produce the flux of nitrogen atoms required by either Marten et al. (1993) or Lellouch et al. (1994), primarily because of the presence of a much greater abundance of H_2 which absorbs in the same wavelength range as N_2. Magnetospheric charged particle impact dissociation of N_2 also does not seem adequate, as the power input in the auroral region (10^8–10^9Watts) is too low. Another possibility is for dissociation by galactic cosmic rays (GCRs) which are expected to deposit their energy and produce secondary electrons in the lower stratosphere and upper troposphere ($p<10$ bar). The unit collisional depth for GCRs occurs at an atmospheric column density of about 10^{25} cm^{-2}. The GCR flux-energy spectrum at Neptune (Selesnick and Stone 1991) is such that most of the N_2 dissociation, and subsequent HCN production, occurs in the 0.1 to 30 mbar range (Atreya et al. 1992). Following the suggestion of Atreya et al. (1992), Lellouch et al. (1994) have modeled the HCN production resulting from GCR impact on N_2; N-atom production profiles were calculated using a simplified GCR ionization rate expression developed by Moses et al. (1992). The derived required N_2 mixing ratio, 0.003 to 0.017, is somewhat uncertain owing to uncertainties in the K value and NH chemistry, but suggests that GCRs could indeed provide a significant fraction of the observed HCN but not likely all of it unless the conversion of N to HCN is very efficient.

Although CO may be produced by reaction between oxygen or oxygen bearing molecules (H_2O, OH, etc.) and the products of methane photochemistry (CH_2, CH_3, C_2H_2, C_3H_2, etc.), it does not appear to be the origin of CO on Neptune (Atreya et al. 1992; Marten et al. 1993). In principle, water can be brought into the upper atmosphere of Neptune through meteoroid ablation; the resulting CO mixing ratio, however, would be far less than the observed value of $\sim 10^{-6}$ (Moses 1992). The same mechanism, i.e., reactions between

H_2O or OH and hydrocarbons, would also produce CO on Uranus, where it has not been detected, and it would produce at least 100 times more CO on Jupiter and Saturn than observed there, considering the possible range in water fluxes from ablating meteorites, rings and moons, and the upper atmospheric temperatures of these planets (Atreya et al. 1992; Marten et al. 1993). Direct migration of CO from Triton is ignorably weak. Finally, an extraplanetary source of CO would result in a gradient in its mixing ratio between the troposphere and stratosphere that has been ruled out by observations. Thus, it appears certain that CO has an intrinsic source on Neptune, as is the case at Jupiter and Saturn (Noll et al. 1988; Noll and Larson 1990). The absence of detectable amounts of CO and HCN in the upper atmosphere of Uranus can be attributed to the sluggishness of convection in its interior, which would severely limit the transport of minor species (N_2 in the case of HCN) to the observable part of the atmosphere.

There is another consideration which is important to keep in mind: that cosmogonic and chemical kinetic considerations favor N_2 as the stable form for nitrogen and CO for carbon (rather than NH_3 and CH_4) everywhere in the solar nebula. The relatively short lifetime of the solar nebula (<30 Myr) is not long enough to attain a state of chemical equilibrium, in which the N_2 and CO originally present in the interstellar cloud would be reduced to NH_3 and CH_4. At the relatively high pressure of the giant planet (Jupiter and Saturn) subnebula and the high pressures and temperatures prevalent in the interiors of Jupiter and Saturn, such conversion can and does occur. In the colder and smaller outer planets and their satellites such processing would be inhibited, allowing some or all nitrogen to remain N_2 and at least some CO to remain CO. This implies that N_2 and CO should be present in the interior of Neptune and Uranus and on other bodies formed in their vicinity. The recent detection of N_2 and CO on Pluto (Owen et al. 1993) and Triton (Cruikshank et al. 1993) supports this hypothesis. The presence of CO and N_2 (or HCN) in the upper troposphere and stratosphere of Neptune, but not of Uranus, has far reaching implications for the accretion, interior structure, and the chemical kinetics of certain key processes in the interiors of these planets. These issues are discussed elsewhere (see the Chapter by Gautier et al.).

V. UPPER ATMOSPHERE

Information regarding the upper atmospheric structure on Neptune is still fragmentary. A limited amount of insight is afforded by the groundbased stellar occultation results, and there are relevant data sets from the Voyager RSS and UVS instruments. The stellar occultation studies were described in Sec. II.A; these are of limited usefulness for pressures $p<1$ μbar owing to the sensitivity of the inversions to measurement uncertainties and imposed initial conditions. The RSS occultations resolved electron density profiles which indicate plasma temperatures ~1000 K above 1000 km altitude and also exhibit strong spikes similar to those observed during the radio occultations of the

other giant planets (Tyler et al. 1989; Lindal 1992). The UVS measurements (Broadfoot et al. 1989) are our primary source of information on the upper atmosphere. Particle-induced emissions were observed, the EUV dayglow (He 584 Å) was measured, and the solar occultation experiments have yielded an estimate of the upper thermospheric temperature at the ingress latitude. However, current modeling capabilities are not such as to allow a useful melding of the RSS and UVS data sets, while the UVS data generally suffer from poor signal-to-noise ratios.

A. Upper Atmosphere Thermal Structure

Results of the preliminary analysis of the UVS ingress solar occultation data were presented by Broadfoot et al. (1989), indicating an upper thermospheric ($p \sim 10^{-5}$ μbar) temperature of ~750 K (Fig. 1) and a temperature of 250 K near 10^{-2} μbar from analysis of absorptions in the Lyman and Werner H_2 band systems. The UVS data at wavelengths below 800 Å (i.e., wavelengths corresponding to the H_2 ionization continuum), which probe the upper thermosphere, have yet to be analyzed in detail, although Yelle et al. (1993) suggested a revised exospheric temperature of 550 K. Difficulties with modeling the H_2 electronic band absorptions in the ingress and egress data were discussed in Sec. II.C.

The thermosphere of Neptune, like those of the other Jovian planets, is surprisingly hot. The temperature rise at the base of the thermosphere amounts to roughly 500 K. In a classical model of a thermosphere the temperature rise is caused by downward conduction of energy deposited at high altitudes by absorption of solar EUV radiation. A 400 K temperature rise over 500 km implies a downward heat flux of 0.1 erg cm^{-2} s^{-1} while the solar energy available to heat the thermosphere is $<10^{-3}$ erg cm^{-2} s^{-1}. Thus, heating by solar EUV fails completely to explain the observations and the apparent heating must be due to other causes.

Neptune's hot thermosphere was not unexpected because Voyager found apparently similar phenomena on Jupiter, Saturn, and Uranus. As yet, no satisfactory explanation for the thermospheric structure on these planets has been offered but we can make some general conclusions from the observations: (1) There is no apparent correlation with heliospheric distance or, equivalently, solar input. Uranus is nearly as warm as Jupiter and Neptune only slightly less so; (2) there is no apparent correlation with the strength of the intrinsic planetary magnetic field; (3) There does appear to be a correlation with the strength of vertical mixing as characterized by the eddy diffusion coefficient. Considering for the moment only Saturn, Uranus, and Neptune, we note that Saturn has the largest eddy coefficient and the lowest thermospheric temperature, Uranus the lowest eddy coefficient and highest thermospheric temperature, and Neptune is intermediate to both cases. The intense aurora on Jupiter could play a role in the thermospheric energy balance of that planet, even at low latitudes, and therefore Jupiter might not follow trends evident on the other planets. If there is a physical mechanism behind the correlation

of exospheric temperatures and eddy mixing rates it is not obvious. Vigorous eddy mixing will carry hydrocarbons to higher altitudes implying reduced exospheric temperatures as observed, but this effect is included in the calculations demonstrating the "energy crisis" and therefore does not solve the problem even though the trend is in the right direction.

Some prior work has suggested that the high thermospheric temperatures are related to large ultraviolet emission rates observed on the outer planets (Shemansky 1985; Shemansky and Smith 1986). This hypothesis can be ruled out. The ultraviolet emission rates vary to high accuracy as the inverse square of heliocentric distance (Broadfoot et al. 1989; Yelle et al. 1987). The thermospheric temperatures on the outer planets show no such trend. In fact, it is easy to show that the thermospheric heating implied by the observed ultraviolet emission rates on Neptune are insignificant. This also holds true for Uranus (Strobel et al. 1991). Clarke et al. (1987) suggested that plasma instabilities could accelerate photoelectrons and produce copious ultraviolet emissions. There are some physical problems with the proposed mechanism that are discussed by Strobel et al. (1991) but even ignoring those the hypothesis does not consistently explain the observations because of the lack of correlation between thermospheric heating and ultraviolet emission rates discussed above.

B. He 584 Å Dayglow

For the H_2-He atmospheres of the outer planets, the He 584 Å dayglow brightness depends on the helium mixing ratio deep in the atmosphere, the eddy mixing coefficient near the homopause, the temperature profile, and the solar flux and line width. Measurement and analysis of this emission at Neptune can serve as a consistency check on some of these parameters derived by other means. The He 584 Å dayglow is excited by resonant scattering of the solar line. Because H_2 absorbs at this wavelength, only helium above an optical depth $\tau \sim 1$ in H_2 contributes to the dayglow. The amount of He above $\tau \sim 1$, and hence the dayglow, increases with the He mixing ratio in the mixed atmosphere and with the eddy mixing coefficient K. He 584 Å dayglow has been measured from all the outer planets except Uranus. Because eddy mixing on Uranus is weak, there is too little He above the $\tau = 1$ level to create a measurable glow. Details of measurements and modeling techniques for Jupiter are given by Carlson and Judge (1971,1976) and McConnell et al. (1981), and for Saturn by Sandel et al. (1982). The observations and analysis for Neptune have been described by Parkinson et al. (1990).

Parkinson et al. inferred a latitudinally averaged He 584 Å dayglow brightness of $0.34^{+0.2}_{-0.15}$ R. The large uncertainty reflects the weak signal and the relatively large background. Their analysis was based on the initial atmospheric model of Broadfoot et al. (1989) with an exospheric temperature of 750 K. The value of K was assumed to be independent of altitude. Using a sophisticated radiative transfer model (Gladstone 1982,1988) and careful estimates of the solar flux and line width at 584 Å, they computed the expected

dayglow brightness as a function of the product $f(\mathrm{He})K$, where $f(\mathrm{He})$ here refers to the mole fraction in the mixed atmosphere. The brightness plotted in this way was found to be nearly independent of $f(\mathrm{He})$, so this parameter value must be taken from other work. Comparing these curves to the measured brightness and its uncertainty, Parkinson et al. inferred $f(\mathrm{He})K \sim 10^7$ $\mathrm{cm^2\,s^{-1}}$, with upper and lower bounds of 3×10^6 and 9×10^7 $\mathrm{cm^2\,s^{-1}}$. The reference value of $f(\mathrm{He}) = 0.19$ (Conrath et al. 1991*a*) implies $K_h \sim 5 \times 10^7$ $\mathrm{cm^2\,s^{-1}}$, with bounds of 6×10^6 and 1.6×10^8 $\mathrm{cm^2\,s^{-1}}$. These uncertainty bounds do not include a contribution from the uncertainty in the solar flux and line width. Including "worst case" uncertainties in these parameters would change the values quoted above by ~50%.

C. Aurora and Photoelectron-Excited Emissions

The offset and 45° tilt of Neptune's magnetic dipole from the spin axis, combined with the 29° tilt of the spin axis to the ecliptic plane, lead to a magnetic configuration that differs in important ways from others that we have had opportunity to study. In particular, for certain rotation phases of Neptune, large areas of the dark side are magnetically conjugate to the daylit hemisphere. Photoelectrons from the day side can then excite emissions in the night atmosphere. A classical aurora near the magnetic poles is probably present as well.

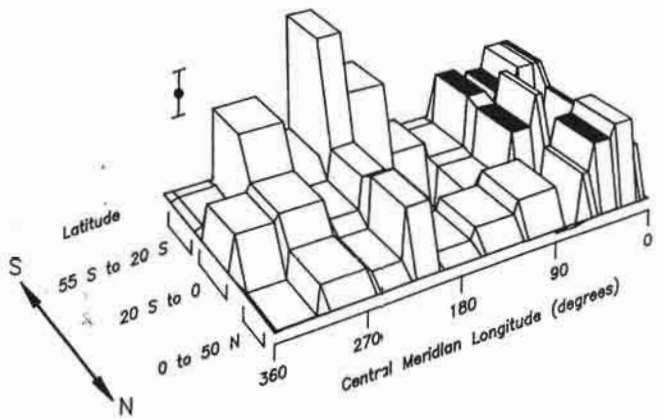

Figure 17. Latitude-longitude map of the relative emission brightness in H_2 bands (96.7–111.5 nm) from Neptune's dark hemisphere measured by the Voyager UVS (Sandel et al. 1990). Two distinct emission regions are evident: a diffuse emission extending over all three latitude bins centered near 30°W longitude and a more localized emission in the southern latitude bin near 240°W longitude. Latitudinal ranges shown are approximate. Typical 1-σ uncertainties are indicated by the single error bar.

Two distinct regions of weak emission have been identified in UVS observations of the night side of Neptune (Fig. 17). Sandel et al. (1990) analyzed data from a mapping sequence in which the UVS slit was scanned repeatedly over the central meridian as the planet turned by more than a complete revolution beneath it. After eliminating measurements that included emission from the sunlit crescent or the sky background, they divided the remaining range of latitudes, from 55°S to 50°N, into three bins. The map derived from these data shows emission from two regions. The first is a diffuse region that extends over all three latitude bins at roughly equal intensity, and extends over longitudes of 0° to 60°W. The emission spectrum is of low quality because the emission is so weak, but it is consistent with H_2 band emissions. The brightness, averaged over the field of view and integrated over the optimum wavelength range (967 to 1115 Å) for detecting H_2 bands is ~2.5 R. Sandel et al. estimated that the emission extends over about 13% of the surface of the planet, and computed a value for the radiated power of about 6×10^7 W. The second region is more localized in both longitude and latitude. It is confined mainly to the southern-most latitude bin near 240°W. Although its brightness of about 5 R is higher, the integration time is lower; hence the spectrum is poorer than that from the first region but also seems consistent with H_2 band emission. For an estimated emitting area of 2% of the surface, the emitted power is 2×10^7 W.

Electron excitation of an H_2 atmosphere produces H Lyman α as well as H_2 band emissions, but the expected H Lyman α brightness is below the detection threshold set by other sources of H Lyman α that were within the field. These included the diffuse H Lyman α background excited over the planet by rescattering of sky background (LISM) H Lyman α (Yelle and Sandel 1986), and direct sky background entering the occultation port of the UVS instrument.

The wide range of latitudes spanned by the diffuse emission is not consistent with usual auroral morphology. Two alternative models for the diffuse emissions have been put forth (Sandel et al. 1990; Cheng 1990*b*). Sandel et al. suggested that the diffuse emissions are excited by precipitating photoelectrons from the magnetically conjugate sunlit hemisphere. As seen from Voyager in the post-encounter period, the emissions appear at longitudes having magnetic conjugate points on the sunlit side. Generally speaking, the emissions should be absent at other rotation phases, where this day-night connection is also absent. This argument was based on a simple picture of an offset tilted dipole magnetic field. Recent field-line tracing using a more realistic magnetic field model has confirmed the early picture, and also shows a region of connection near the southern bright spot.

A viable model for the diffuse emission must not only match the observed morphology but also supply the needed energy. Sandel et al. argued that an efficiency of about 0.5% is needed in the conversion from solar flux and suggested that such an efficiency is not unreasonable. Scaling photoelectron fluxes measured above Earth's atmosphere also indicates that the required

energy may be available. No detailed model calculations have been done, however.

The second model advanced to account for the diffuse emission is based on the large offset and tilt of Neptune's magnetic dipole, which create a large region of anomalously low surface magnetic field strength (Cheng 1990*b*). Trapped particles drifting around the planet precipitate into the atmosphere when they encounter this weak field region. The anomaly extends from the north magnetic pole (51°N, 48°W) to a point on the magnetic equator at 38°S, 167°W. In this model, westward-drifting electrons precipitate at the eastern edge of this region, exciting the diffuse emission. Eastward-drifting protons precipitate on the other side, possibly contributing to the enhanced ultraviolet emission near 240°W. Energetic particle signatures support the idea of such a precipitation pattern, and show that the precipitating particles have sufficient energy to account for the observed emission (Cheng 1990*b*). While the morphology predicted by anomaly driven precipitation is generally consistent with that observed, it differs in detail. The model predicts more variation with latitude in the longitude of the diffuse emission than is observed. However, the signal-to-noise ratio of the ultraviolet map is rather low and it is not clear that the observations are inconsistent with this model.

The localized region in the south is near the magnetic pole and may be a classical aurora. This interpretation is supported by observations of trapped particles (Krimigis et al. 1989) and nonthermal radio emissions (Gurnett et al. 1989; Warwick et al. 1989) normally associated with auroral particle acceleration. A brighter aurora would be expected at the other pole owing to the weaker field strength there. Unfortunately the 51°N latitude of that pole places it at the edge of the area mapped by the UVS and its position near the limb may have further reduced its apparent brightness. Thus we lack a reliable measurement of possible auroral emission there. To evaluate possible power sources, it is reasonable to assume that the total radiated power is approximately twice that observed for the better-observed southern spot, that is, about 5×10^7W.

For an efficiency of 3%, the magnetospheric input power must be $\sim 1.5 \times 10^9$W. Broadfoot et al. (1989) described a mechanism for deriving this power from Neptune's rotational energy using the medium of mass loading in "plasma arcs" associated with mass injection from Triton. These ideas were further developed by Hill and Dessler (1990) and Sandel et al. (1990). Their mechanism requires a mass loading rate of about 1 kg s^{-1}. Models of the atmosphere of Triton suggest a total H+N loss rate of about half this level (Chapter by Strobel and Summers).

An alternative model (Cheng 1989,1990*a*) invokes an external source, the solar wind, to power the aurora. Field-aligned currents and potential drops above the polar caps are the agents by which the energy is transferred to the atmosphere. The required efficiency for converting solar wind power is about 0.3%, or about 1/3 of the value observed at Earth. Thus two distinct mechanisms are at hand to account for both the aurora and the diffuse emission.

Given the low signal-to-noise ratio of the available data, it is difficult to use the observations to choose between them.

To assess the importance of the auroral power for the global atmospheric structure, we compare it to the power deposited by the ionizing solar flux. The globally averaged solar flux at Neptune is $\sim 10^{-3}$ erg cm^{-2} s^{-1}, and the maximum value, for an overhead Sun, is $\sim 4 \times 10^{-3}$ erg cm^{-2} s^{-1}. Using the brightnesses and areas given by Sandel et al., we estimate the input power for the localized emission to be about 1×10^{-3} erg cm^{-2} s^{-1}, comparable to the solar flux. The diffuse emission is about half as bright. In terms of total power integrated over the surface, the auroral input power is about 2% (for the localized emission) and 7% (for the diffuse emission) of the solar input. Thus the aurora may be important locally, but are not likely to influence the structure of the atmosphere on a planetary scale.

D. Ionosphere

The Voyager 2 ionospheric measurements at Neptune were carried out by the radio occultation technique using the spacecraft's tracking carrier frequencies at S and X bands (2.3 GHz or 13 cm, and 8.4 GHz or 3.6 cm, respectively; Tyler et al. 1989); these measurements completed the acquisition of electron concentration profiles for the ionospheres of all the major planets. The electron concentration profiles for Neptune are shown in Fig. 18. The ingress occultation data on the ionosphere were acquired near 62°N latitude, 227°E longitude, the egress occultation data near 45°S latitude, 131°E longitude (Lindal 1992). Both ingress and egress electron concentration measurements occurred at the morning terminator. An extensive ionosphere, with electron concentrations greater than 100 cm^{-3}, was detected up to 5000 km altitude (measured from the 1 bar pressure level). The data beyond 2500 km, however, are suspect because of the effects of variations in the terrestrial ionosphere and interplanetary medium through which the radio signal traverses.

Both ingress and egress measurements yield electron concentrations of the order of 1 to 2×10^3cm^{-3} at an altitude of 1400 km. A well defined sharp layer with an electron concentration of 7×10^3cm^{-3} is evident at $\sim$1200 km in the egress data. Several other layer-like features are seen below 1000 km. Not all of these necessarily represent real ionospheric layers; some may be due to unresolved multipath propagation (Eshleman et al. 1977) arising in genuine layers. Similar features were seen in the lower ionospheres of Jupiter, Saturn, and Uranus. The topside plasma scale height is around 1800±300 km and the corresponding electron/ion temperature is 950±160 K (Tyler et al. 1989), taking H^+ to be the major topside ion and assuming equilibrium between electron, ion, and neutral temperatures. The exospheric neutral temperature at altitudes above 2000 km was found to be $\sim$750 K (Broadfoot et al. 1989). Within the range of uncertainties the ion and neutral temperatures seem similar, giving support to the identification of the topside ion as H^+. Furthermore, unlike Jupiter and Saturn, the inner magnetosphere at Neptune (and Uranus) is populated mainly by H^+, presumably of ionospheric

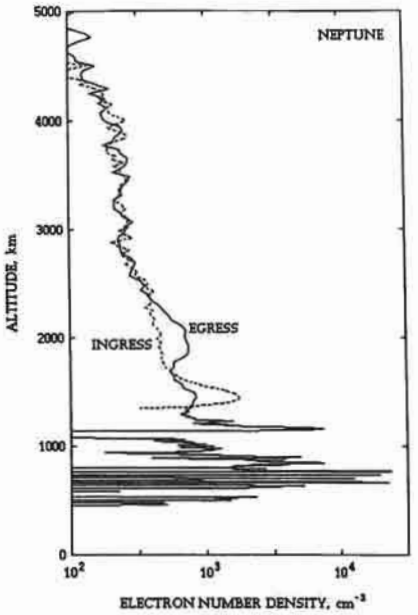

Figure 18. Vertical distributions of electron density in Neptune's ionosphere measured during the Voyager 2 RSS occultations. Both ingress and egress profiles were obtained near the morning terminator. Altitudes are with respect to the 1 bar level (figure taken from Lindal 1992).

origin. The former planets also have H_2^+ and H_3^+ (among other species) present in their magnetospheres.

Despite the relatively small solar ionizing flux incident at Neptune, only 3% of that at Jupiter, its ionosphere is generated primarily by solar EUV radiation. Even in the auroral region of Neptune, the magnetospheric power input is relatively small, 10^8 to 10^9 W, compared with more than 10^{13} W into Jupiter's auroral region. Thus one does not expect a large latitudinal variation in the behavior of Neptune's ionosphere. In a simplified chemical scheme for the ionosphere, the production of ions via solar photoionization is followed by charge transfer and ion loss processes. In Neptune's ionosphere the following processes are expected to be important:

Ion production

$$H_2 + h\nu \text{ (or } e^-) \rightarrow H_2^+ + e^- \text{ (or } 2e^-) \quad (\geq 90\%) \tag{7}$$

$$\rightarrow H^+ + H + e^- \text{ (or } 2e^-) \tag{8}$$

$$H + h\nu \text{ (or } e^-) \rightarrow H^+ + e^- \text{ (or } 2e^-) \tag{9}$$

$$C_nH_m + h\nu \text{ (or } e^-) \rightarrow C_nH_m{}^+ + e^- \text{ (or } 2e^-) \tag{10}$$

with Reaction (9) important in the topside ionosphere where $[H] > [H_2]$ and Reaction (10) important in the middle and lower stratosphere where hydrocarbon abundances are relatively large;

Charge exchange

$$H_2^+ + H \rightarrow H_2 + H^+ \quad (11)$$

$$H_2^+ + H_2 \rightarrow H_3^+(v = 0) + H \quad (12)$$

$$H^+ + H_2 + M \rightarrow H_3^+(v = 0) + M \quad (13)$$

$$H^+ \text{ (or } H_3^+) + C_nH_m \rightarrow C_nH_m{}^+ + \text{neutrals} \quad (14)$$

with Reaction (11) the main channel near and above the electron density peak ([H]>[H_2]), Reactions (12) and (13) significant in the vicinity of the electron density peak and below (M represents background atmosphere), and Reaction (14) significant in the middle and lower stratosphere where C_nH_m abundances are relatively large; and

Ion loss

$$X^+ \text{ (or } XY^+) + e^- \rightarrow \text{neutrals} \quad (15)$$

i.e., the eventual loss of all ions is by dissociative or radiative recombination. (A detailed and complete discussion of ionospheric chemistry on the major planets is given in Atreya [1986].) The low magnetospheric power input does not permit production of large quantities of vibrationally excited H_2. On Jupiter (and, presumably, on Saturn also) a reaction between H^+ and H_2 ($v \geq 4$) can occur, converting the long-lived H^+ ions to short-lived H_2^+. (H_2^+ would then immediately react with H_2 to form the short-lived terminal ion H_3^+ at appropriate altitudes.) As mentioned earlier, there is indirect evidence that H^+ is the major topside ion at Neptune. In fact, H^+ should remain the major ion below the peak; however, significant concentrations of H_3^+ just below the peak and of hydrocarbon ions in the deep atmosphere below the tropopause are expected. A preliminary pre-Voyager model of the ionosphere of Neptune was developed by Atreya (1984) along the lines of his earlier models for Jupiter and Saturn. This model predicted a peak electron concentration of 1000 to 3000 cm^{-3} at an atmospheric density level of $10^9 cm^{-3}$ (which occurs at around 1400 km altitude), in agreement with the results obtained from the Voyager 2 ingress and egress occultation measurements at Neptune. The sharp ionization layer at 1200 km is most likely reminiscent of terrestrial sporadic E-type layering of metallic ions caused by wind shears, as was suggested for Jupiter (Atreya et al. 1974). The metallic ions are expected to be introduced into Neptune's ionosphere by meteorites ablating in its atmosphere. Unlike Jupiter, there is no magnetospheric source of appropriate ions at Neptune (the Io torus can supply sodium and sulfur ions to Jupiter, which may also cause ionospheric layering [Atreya et al. 1974; Chen 1981]). Finally, modeling by Capone et al. (1977), taking into consideration the penetration of galactic cosmic rays, indicates that heavy hydrocarbon ions with concentrations as large as $10^4 cm^{-3}$ are produced near and below the tropopause (~100 mbar) of Neptune. Thus large electron concentrations are expected owing to this process several hundred kilometers below the solar EUV-generated ionosphere.

Acknowledgments. We would like to acknowledge useful comments from F. Herbert, D. Hinson, D. Hunten, J. Lyons, and F. Roques.

REFERENCES

Appleby, J. F. 1986. Radiative-convective equilibrium models of Uranus and Neptune. *Icarus* 65:383–405.

Appleby, J. F. 1990. CH_4 nonlocal thermodynamic equilibrium in the atmospheres of the giant planets. *Icarus* 85:355–379.

Atreya, S. K. 1984. Aeronomy. In *Uranus and Neptune*, ed. J. T. Bergstralh, NASA CP-2330, pp. 55–88.

Atreya, S. K. 1986. *Atmospheres and Ionospheres of the Outer Planets and Their Satellites* (New York: Springer-Verlag).

Atreya, S. K., Donahue, T. M., and McElroy, M. B. 1974. Jupiter's ionosphere: Prospects for Pioneer 10. *Science* 184:154–156.

Atreya, S. K., Owen, T. C., Gautier, D., and Marten, A. 1992. HCN and CO on Neptune: An intrinsic origin. *Bull. Amer. Astron. Soc.* 24:972 (abstract).

Baines, K. H., and Hammel, H. B. 1994. Clouds, hazes, and the stratospheric methane abundance ratio in Neptune. *Icarus* 109:20–39.

Baines, K. H., and Smith, W. H. 1990. The atmospheric structure and dynamical properties of Neptune derived from ground-based and IUE spectrophotometry. *Icarus* 85:65–108.

Baum, W. A., and Code, A. D. 1953. A photometric observation of the occultation of σ Arietis by Jupiter. *Astron. J.* 58:108–112.

Bézard, B. 1989. Seasonal thermal structure in the atmospheres of the giant planets. *Adv. Space Res.* 10:89–98.

Bézard, B., Romani, P. N., Conrath, B. J., and Maguire, W. C. 1991. Hydrocarbons in Neptune's stratosphere from Voyager infrared observations. *J. Geophys. Res.* 96:18961–18975.

Bishop, J., Atreya, S. K., Herbert, F., and Romani, P. 1990. Reanalysis of Voyager 2 UVS occultations at Uranus: Hydrocarbon mixing ratios in the equatorial stratosphere. *Icarus* 88:448–464.

Bishop, J., Atreya, S. K., Romani, P. N., Sandel, B. R., and Herbert, F. 1992. Voyager 2 ultraviolet spectrometer solar occultations at Neptune: Constraints on the abundance of methane in the stratosphere. *J. Geophys. Res.* 97:11681–11694.

Broadfoot, A. L., Sandel, B. R., Shemansky, D. E., Atreya, S. K., Donahue, T. M., Moos, H. W., Bertaux, J. L., Blamont, J. E., Ajello, J. M., Strobel, D. F., McConnell, J. C., Dalgarno, A., Goody, R., McElroy, M. B., and Yung, Y. L. 1977. Ultraviolet spectrometer experiment for the Voyager mission. *Space Sci. Rev.* 21:183–205.

Broadfoot, A. L., Atreya, S. K., Bertaux, J. L., Blamont, J. E., Dessler, A. J., Donahue, T. M., Forrester, W. T., Hall, D. T., Herbert, F., Holberg, J. B., Hunten, D. M., Krasnopolsky, V. A., Linick, S., Lunine, J. I., McConnell, J. C., Moos, H. W., Sandel, B. R., Schneider, N. M., Shemansky, D. E., Smith, G. R., Strobel, D. F., and Yelle, R. V. 1989. Ultraviolet spectrometer observations of Neptune and Triton. *Science* 246:1459–1466.

Caldwell, J., Wagener, R., and Fricke, K.-H. 1988. Observations of Neptune and Uranus below 2000 Å with the IUE. *Icarus* 74:133–140.

Capone, L. A., Whitten, R. C., Prasad, S. S., and Dubach, J. 1977. The ionospheres of Saturn, Uranus, and Neptune. *Astrophys. J.* 215:977–983.

Carlson, R. W., and Judge, D. L. 1971. The extreme ultraviolet dayglow of Jupiter. *Planet. Space Sci.* 19:327–343.

Carlson, R. W., and Judge, D. L. 1976. Pioneer 10 ultraviolet photometer observations of Jupiter: The helium to hydrogen ratio. In *Jupiter*, ed. T. Gehrels (Tucson: Univ. of Arizona Press), pp. 418–440.

Chen, R. H. 1981. Studies of Jupiter's lower ionospheric layers. *J. Geophys. Res.* 86:7792–7794.

Cheng, A. F. 1989. Magnetosphere of Neptune: Auroral zone field-aligned potential drops? *Geophys. Res. Lett.* 16:953–956.

Cheng, A. F. 1990*a*. Triton torus and Neptune aurora. *Geophys. Res. Lett.* 17:1669–1672.

Cheng, A. F. 1990*b*. Global magnetic anomaly and aurora of Neptune. *Geophys. Res. Lett.* 17:1697–1700.

Clarke, J. T., Hudson, M. K., and Yung, Y. L. 1987. The excitation of the far ultraviolet electroglow emissions on Uranus, Saturn, and Jupiter. *J. Geophys. Res.* 92:15139–15147.

Conrath, B. J., Flasar, F. M., Hanel, R., Kunde, V., Maguire, W., Pearl, J., Pirraglia, J., Samuelson, R., Gierasch, P., Weir, A., Bézard, B., Gautier, D., Cruikshank, D., Horn, L., Springer, R., and Shaffer, W. 1989. Infrared observations of the Neptunian system. *Science* 246:1454–1459.

Conrath, B. J., Gierasch, P. J., and Leroy, S. S. 1990. Temperature and circulation in the stratosphere of the outer planets. *Icarus* 83:255–281.

Conrath, B. J., Gautier, D., Lindal, G. F., Samuelson, R. E., and Shaffer, W. A. 1991*a*. The helium abundance of Neptune from Voyager measurements. *J. Geophys. Res.* 96:18907–18919.

Conrath, B. J., Flasar, F. M., and Gierasch, P. J. 1991*b*. Thermal structure and dynamics of Neptune's atmosphere from Voyager measurements. *J. Geophys. Res.* 96:18931–18939.

Conrath, B. J., Gautier, D., Owen, T. C., and Samuelson, R. E. 1993. Constraints on N_2 in Neptune's atmosphere from Voyager measurements. *Icarus* 101:168–172.

Courtin, R., Gautier, D., and Lacombe, A. 1979. Indications of supersaturated stratospheric methane in Neptune from its atmospheric thermal profile. *Icarus* 37:236–248.

Cruikshank, D. P., Roush, T. L., Owen, T. C., Geballe, T. R., de Bergh, C., Schmitt, B., Brown, R. H., and Bartholomew, M. J. 1993. Ices on the surface of Triton. *Science* 261:742–745.

Danielson, R. E. 1977. The structure of the atmosphere of Uranus. *Icarus* 30:462–478.

Danielson, R. E., Cochran, W. D., Wannier, P. G., and Light, E. S. 1977. A saturation model of the atmosphere of Uranus. *Icarus* 31:97–109.

Dunkerton, T. J. 1989. Theory of internal gravity wave saturation. *Pure Appl. Geophys.* 130:373–397.

Eshleman, V. R., Tyler, G. L., Anderson, J. D., Fjeldbo, G., Levy, G. S., Wood, G. E., and Croft, T. A. 1977. Radio science investigations with Voyager. *Space Sci. Rev.* 21:207–232.

Freeman, K. C., and Lyngå, G. 1970. Data for Neptune from occultation observations. *Astrophys. J.* 160:767–780.

French, R. G., and Gierasch, P. J. 1974. Waves in the Jovian upper atmosphere. *J. Atmos. Sci.* 31:1707–1712.

French, R. G., and Lovelace, R. V. E. 1983. Strong turbulence and atmospheric waves

in stellar occultations. *Icarus* 56:122–146.

French, R. G., Elliot, J. L., and Gierasch, P. J. 1978. Analysis of stellar occultation data: Effects of photon noise and initial conditions. *Icarus* 33:186–202.

French, R. G., Elias, J. H., Mink, D. J., and Elliot, J. L. 1983. The structure of Neptune's upper atmosphere: The stellar occultation of 24 May 1981. *Icarus* 55:332–336.

French, R. G., Melroy, P. A., Baron, R. L., Dunham, E. W., Meech, K. J., Mink, D. J., Elliot, J. L., Allen, D. A., Ashley, M. C. B., Freeman, K. C., Erickson, E. F., Goguen, J., and Hammel, H. B. 1985. The 1983 June 15 occultation by Neptune. II. The oblateness of Neptune. *Astron. J.* 90:2624–2638.

Friedson, A. J., and Orton, G. S. 1992. The zonally symmetric component of Neptune's circulation. Neptune and Triton, Jan. 6–10, Tucson, Ariz., Abstract book, p. 24.

Garcia, R. R., and Solomon, S. 1985. The effect of breaking gravity waves on the dynamics and chemical composition of the mesosphere and lower thermosphere. *J. Geophys. Res.* 90:3850–3868.

Gillett, F. C., and Rieke, G. H. 1977. 5–20 micron observations of Uranus and Neptune. *Astrophys. J. Lett.* 218:141–144.

Gladstone, G. R. 1982. Radiative transfer with partial frequency redistribution in inhomogeneous atmospheres: Application to the Jovian aurora. *J. Quant. Spectrosc. Radiat. Transfer* 27:545–556.

Gladstone, G. R. 1988. UV resonance line dayglow emissions on Earth and Jupiter. *J. Geophys. Res.* 93:14623–14630.

Guilloteau, S., Dutrey, A., Marten, A., and Gautier, D. 1993. CO in the troposphere of Neptune: Detection of the J = 1–0 line in absorption. *Astron. Astrophys.* 279:661–667.

Gurnett, D. A., Kurth, W. S., Poynter, R. L., Granroth, L. J., Cairns, I. H., Macek, W. M., Moses, S. L., Coroniti, F. V., Kennel, C. F., and Barbosa, D. D. 1989. First plasma wave observations at Neptune. *Science* 246:1494–1498.

Hammel, H. B., Young, L. A., Hackwell, J., Lynch, D. K., Russell, R., and Orton, G. S. 1992. Variability of Neptune's 12.2-μm ethane emission feature. *Icarus* 99:347–352.

Hanel, R., Conrath, B., Gautier, D., Gierasch, P., Kumar, S., Kunde, V., Lowman, P., Maguire, W., Pearl, J., Pirraglia, J., Ponnamperuma, C., and Samuelson, R. 1977. The Voyager infrared spectroscopy and radiometry investigation. *Space Sci. Rev.* 21:129–157.

Herbert, F., Sandel, B. R., Yelle, R. V., Holberg, J. B., Broadfoot, A. L, Shemansky, D. E., Atreya, S. K., and Romani, P. N. 1987. The upper atmosphere of Uranus: EUV occultations observed by Voyager 2. *J. Geophys. Res.* 92:15093–15109.

Hildebrand, R. H., Loewenstein, R. F., Harper, D. A., Orton, G. S., Keene, J., and Whitcomb, S. E. 1985. Far-infrared and submillimeter brightness temperatures of the giant planets. *Icarus* 64:64–87.

Hill, T. W., and Dessler, A. J. 1990. Convection in Neptune's magnetosphere. *Geophys. Res. Lett.* 17:1677–1680.

Hinson, D. P., and Magalhães, J. A. 1991. Equatorial waves in the stratosphere of Uranus. *Icarus* 94:64–91.

Hinson, D. P., and Magalhães, J. A. 1993. Inertio-gravity waves in the atmosphere of Neptune. *Icarus* 105:142–161.

Holton, J. R., and Schoeberl, M. R. 1988. The role of gravity wave generated advection and diffusion in transport of tracers in the mesosphere. *J. Geophys. Res.* 93:11075–11082.

Hubbard, W. B., Frecker, J. E., Gehrels, J.-A., Gehrels, T., Hunten, D. M., Lebofsky, L. A., Smith, B. A., Tholen, D. J., Vilas, F., Zellner, B., Avey, H. P., Mottram, K., Murphy, T., Varnes, B., Carter, B., Nielsen, A., Page, A. A., Fu, H. H., Wu, H. H.,

Kennedy, H. D., Waterworth, M. D., and Reitsema, H. J. 1985. Results from observations of the 15 June 1983 occultation by the Neptune system. *Astron. J.* 90:655–667.

Hubbard, W. B., Nicholson, P. D., Lellouch, E., Sicardy, B., Brahic, A., Vilas, F., Bouchet, P., McLaren, R. A., Millis, R. L., Wasserman, L. H., Elias, J. H., Matthews, K., McGill, J. D., and Perrier, C. 1987. Oblateness, radius, and mean stratospheric temperature of Neptune from the 1985 August 20 occultation. *Icarus* 72:635–646.

Hubbard, W. B., Lellouch, E., Sicardy, B., Brahic, A., Vilas, F., Bouchet, P., McLaren, R. A., and Perrier, C. 1988. Structure of scintillations in Neptune's occultation shadow. *Astrophys. J.* 325:490–502.

Hunten, D. M. 1974. Introduction and summary. In *The Atmosphere of Uranus: The Proceedings of a Workshop held at Ames Research Center September 30, 1974*, ed. D. M. Hunten (Washington, D. C.: U. S. Government Printing Office), pp. 1–7.

Hunten, D. M. 1975. Vertical transport in atmospheres. In *Atmospheres of Earth and the Planets*, ed. B. M. McCormac (Dordrecht: D. Reidel), pp. 59–72.

Hunten, D. M., and Veverka, J. 1976. Stellar and spacecraft occultations by Jupiter: A critical review of derived temperature profiles. In *Jupiter*, ed. T. Gehrels (Tucson: Univ. of Arizona Press), pp. 247–283.

Kostiuk, T., Espenak, F., Romani, P., Zipoy, D., and Goldstein, J. 1990. Ethane abundance on Neptune. *Icarus* 88:87–96.

Kostiuk, T., Romani, P., Espenak, F., and Bézard, B. 1992. Stratospheric ethane on Neptune: Comparison of groundbased and Voyager IRIS retrievals. *Icarus* 99:353–362.

Kovalevsky, J., and Link, F. 1969. Diamètre, applatissement et propriétés optiques de la haute atmosphère de Neptune d'aprés l'occultation de l'étoile BD-17°4388. *Astron. Astrophys.* 2:398–412.

Krimigis, S. M., Armstrong, T. P., Axford, W. I., Bostrom, C. O., Cheng, A. F., Gloeckler, G., Hamilton, D. C., Keath, E. P., Lanzerotti, L. J., Mauk, B. H., and Van Allen, J. A. 1989. Hot plasma and energetic particles in Neptune's magnetosphere. *Science* 246:1483–1489.

Lellouch, E., Hubbard, W. B., Sicardy, B., Vilas, F., and Bouchet, P. 1986. Occultation determination of Neptune's oblateness and stratospheric methane mixing ratio. *Nature* 324:227–231.

Lellouch, E., Romani, P. N., and Rosenqvist, J. 1994. The vertical distribution and origin of HCN in Neptune's atmosphere. *Icarus* 108:112–136.

Lightfoot, P. D., and Pilling, M. J. 1987. Temperature and pressure dependence of the rate constant for the addition of H to C_2H_4. *J. Phys. Chem.* 91:3373–3379.

Lindal, G. F. 1992. The atmosphere of Neptune: An analysis of radio occultation data acquired with Voyager 2. *Astron. J.* 103:967–982.

Lindal, G. F., Lyons, J. R., Sweetnam, D. N., Eshleman, V. R., Hinson, D. P., and Tyler, G. L. 1990. The atmosphere of Neptune: Results of radio occultation measurements with the Voyager 2 spacecraft. *Geophys. Res. Lett.* 17:1733–1736.

Lindzen, R. S. 1971. Tides and gravity waves in the upper atmosphere. In *Mesospheric Models and Related Experiments*, ed. G. Fiocco (Dordrecht: D. Reidel), pp. 122-130.

Lindzen, R. S. 1981. Turbulence and stress owing to gravity wave and tidal breakdown. *J. Geophys. Res.* 86:9707–9714.

Lockwood, G. W., and Thompson, D. T. 1991. Solar cycle relationship clouded by Neptune's sustained brightness maximum. *Nature* 349:593–594.

Lunine, J. I., and Hunten, D. M. 1989. Abundance of condensable species at planetary cold traps: The role of moist convection. *Planet. Space Sci.* 37:151–166.

Lyons, J. R., Yung, Y. L., and Allen, M. 1992. Solar control of the upper atmosphere of Triton. *Science* 256:204–206.

Lyons, J. R., Yung, Y. L., and Allen, M. 1993. Photochemistry of the atmosphere and ionosphere of Triton. *Icarus*, submitted.

Macy, W., Jr., and Trafton, L. 1975. Neptune's atmosphere: The source of the thermal inversion. *Icarus* 26:428–436.

Macy, W., Jr., and Sinton, W. 1977. Detection of methane and ethane emission on Neptune but not on Uranus. *Astrophys. J. Lett.* 218:79–81.

Marten, A., Gautier, D., Owen, T., Sanders, D., Tilanus, R. T., Deane, J., and Matthews, H. 1991. First detection of CO and HCN in the atmosphere of Neptune. *Bull. Amer. Astron. Soc.* 23:1164 (abstract).

Marten, A., Gautier, D., Owen, T., Sanders, D. B., Matthews, H. E., Atreya, S. K., Tilanus, R. P. J., and Deane, J. R. 1993. First observations of CO and HCN on Neptune and Uranus at millimeter wavelengths and their implications for atmospheric chemistry. *Astrophys. J.* 406:285–297.

McConnell, J. C., Sandel, B. R., and Broadfoot, A. L. 1981. Voyager U.V. spectrometer observations of He 584 Å dayglow at Jupiter. *Planet. Space Sci.* 29:283–292.

Mordaunt, D. H., Lambert, I. R., Morley, G. P., Ashfold, M. N. R., Dixon, R. N., Western, C. M., Schnieder, L., and Welge, K. H. 1993. Primary product channels in the photodissociation of methane at 121.6 nm. *J. Chem. Phys.* 98:2054–2065.

Moseley, H., Conrath, B., and Silverberg, R. F. 1985. Atmospheric temperature profiles of Uranus and Neptune. *Astrophys. J. Lett.* 292:83–86.

Moses, J. I. 1991. Part II. Photochemistry and Aerosol Formation in Neptune's Atmosphere. Ph.D. Thesis, California Inst. of Technology.

Moses, J. I. 1992. Meteoroid ablation in Neptune's atmosphere. *Icarus* 99:368–383.

Moses, J. I., Allen, M., and Yung, Y. L. 1992. Hydrocarbon nucleation and aerosol formation in Neptune's atmosphere. *Icarus* 99:318–346.

Narayan, R., and Hubbard, W. B. 1988. Theory of anisotropic refractive scintillation: Application to stellar occultations by Neptune. *Astrophys. J.* 325:503–518.

Noll, K. S., and Larson, H. P. 1990. The spectrum of Saturn from 1990 to 2230 cm^{-1}: Abundances of AsH_3, CH_3D, CO, GeH_4, NH_3, and PH_3. *Icarus* 89:168–189.

Noll, K. S., Knacke, R. F., Geballe, T. R., and Tokunaga, A. T. 1988. The origin and vertical distribution of carbon monoxide in Jupiter. *Astrophys. J.* 324:1210–1218.

Orton, G. S., and Appleby, J. F. 1984. Temperature structures and infrared-derived properties of the atmospheres of Uranus and Neptune. In *Uranus and Neptune*, ed. J. T. Bergstralh, NASA CP-2330, pp. 89–155.

Orton, G. S., Tokunaga, A. T., and Caldwell, J. 1983. Observational constraints on the atmospheres of Uranus and Neptune from new measurements near 10 μm. *Icarus* 56:147–164.

Orton, G. S., Griffin, M. J., Ade, P. A. R., Nolt, I. G., Radostitz, J. V., Robson, E. I., and Gear, W. K. 1986. Submillimeter and millimeter observations of Uranus and Neptune. *Icarus* 67:289–304.

Orton, G. S., Aitken, D. K., Smith, C., Roche, P. F., Caldwell, J., and Snyder, R. 1987. The spectra of Uranus and Neptune at 8–14 and 17–23 μm. *Icarus* 70:1–12.

Orton, G. S., Baines, K. H., Caldwell, J., Romani, P., Tokunaga, A. T., and West, R. A. 1990. Calibration of the 7- to 14-μm brightness spectra of Uranus and Neptune. *Icarus* 85:257–265.

Orton, G. S., Lacy, J. H., Achtermann, J. M., Parmar, P., and Blass, W. E. 1992. Thermal spectroscopy of Neptune: The stratospheric temperature, hydrocarbon abundances, and isotopic ratios. *Icarus* 100:541–555.

Owen, T. C., Roush, T. L., Cruikshank, D. P., Elliot, J. L., Young, L. A., de Bergh, C., Schmitt, B., Geballe, T. R., Brown, R. H., and Bartholomew, M. J. 1993. Surface ices and the atmospheric composition of Pluto. *Science* 261:745–748.

Parkinson, C. D., McConnell, J. C., Sandel, B. R., Yelle, R. V., and Broadfoot, A. L. 1990. He 584 Å dayglow at Neptune. *Geophys. Res. Lett.* 17:1709–1712.

Pollack, J. B., Rages, K., Pope, S. K., Tomasko, M. G., Romani, P. N., and Atreya, S. K. 1987. Nature of the stratospheric haze on Uranus: Evidence for condensed hydrocarbons. *J. Geophys. Res.* 92:15037–15065.

Pryor, W. R., West, R. A., Simmons, K. E., and Delitsky, M. 1992. High-phase-angle observations of Neptune at 2650 and 7500 Å: Haze structure and particle properties. *Icarus* 99:302–317.

Richardson, J. D., Belcher, J. W., Zhang, M., and McNutt, R. L., Jr. 1991. Low-energy ions near Neptune. *J. Geophys. Res.* 96:18993–19011.

Romani, P. N., and Atreya, S. K. 1989. Stratospheric aerosols from CH_4 photochemistry in Neptune. *Geophys. Res. Lett.* 16:941–944.

Romani, P. N., Bishop, J., Bézard, B., and Atreya, S. 1993. Methane photochemistry on Neptune: Ethane and acetylene mixing ratios and haze production. *Icarus* 106:442–463.

Roques, F., Sicardy, B., French, R. G., Hubbard, W. B., Barucci, A., Bouchet, P., Brahic, A., Gehrels, J.-A., Gehrels, T., Grenier, I., Lebertre, T., Lecacheux, J., Maillard, J. P., McLaren, R. A., Perrier, C., Vilas, F., and Waterworth, M. D. 1994. Neptune's upper stratosphere, 1983–1990: Ground-based stellar occultation observations III. Temperature profiles. *Astron. Astrophys.* 288:985–1011.

Rosenqvist, J., Lellouch, E., Romani, P. N., Paubert, G., and Encrenaz, T. 1992. Millimeter-wave observations of Saturn, Uranus, and Neptune: CO and HCN on Neptune. *Astrophys. J. Lett.* 392:99–102.

Sandel, B. R., McConnell, J. C., and Strobel, D. F. 1982. Eddy diffusion at Saturn's homopause. *Geophys. Res. Lett.* 9:1077–1080.

Sandel, B. R., Herbert, F., Dessler, A. J., and Hill, T. W. 1990. Aurora and airglow on the night side of Neptune. *Geophys. Res. Lett.* 17:1693–1696.

Selesnick, R. S., and Stone, E. C. 1991. Neptune's cosmic ray cutoff. *Geophys. Res. Lett.* 18:361–364.

Shemansky, D. E. 1985. An explanation for the H Ly α longitudinal asymmetry in the equatorial spectrum of Jupiter: An outcrop of paradoxical energy deposition in the exosphere. *J. Geophys. Res.* 90:2673–2694.

Shemansky, D. E., and Smith, G. R. 1986. The implication for the presence of a magnetosphere on Uranus in the relationship of EUV and radio emission. *Geophys. Res. Lett.* 13:2–5.

Slanger, T. G., and Black, G. 1982. Photodissociative channels at 1216 Å for H_2O, NH_3, and CH_4. *J. Chem. Phys.* 77:2432–2437.

Stoker, C. R. 1986. Moist convection: A mechanism for producing the vertical structure of the Jovian equatorial plumes. *Icarus* 67:106–125.

Stoker, C. R., and Toon, O. B. 1989. Moist convection on Neptune. *Geophys. Res. Lett.* 16:929–932.

Strobel, D. F. 1985. The photochemistry of the atmospheres of the outer planets and their satellites. In *The Photochemistry of Atmospheres: Earth, the Other Planets, and Comets*, ed. J. S. Levine (Orlando: Academic Press), pp. 393–434.

Strobel, D. F., Summers, M. E., Bevilacqua, R. M., DeLand, M. T., and Allen, M. 1987. Vertical constituent transport in the mesosphere. *J. Geophys. Res.* 92:6691–6698.

Strobel, D. F., Summers, M. E., Herbert, F., and Sandel, B. R. 1990. The photochemistry of methane in the atmosphere of Triton. *Geophys. Res. Lett.* 17:1729–1732.

Strobel, D. F., Yelle, R. V., Shemansky, D. E., and Atreya, S. K. 1991. The upper atmosphere of Uranus. In *Uranus*, eds. J. T. Bergstralh, E. D. Miner and M. S. Matthews (Tucson: Univ. of Arizona Press), pp. 65–109.

Summers, M. E., and Strobel, D. F. 1989. Photochemistry of the atmosphere of